A Reduced Basis Method for a PDE-constrained optimization formulation in Discrete Fracture Network flow simulations

(Article begins on next page)

09 April 2024

A Reduced Basis Method for a PDE-constrained optimization formulation in Discrete Fracture Network flow simulations [☆]

S. Berrone[a,b], F. Vicini[a,b,*]

[a]*Dipartimento di Scienze Matematiche, Politecnico di Torino*
Corso Duca degli Abruzzi 24, Torino, 10129, Italy
[b]*Member of the INdAM research group GNCS*

Abstract

In classic Reduced Basis (RB) framework, we propose a new technique for the offline greedy error analysis which relies on a residual-based a posteriori error estimator. This approach is as an alternative to classical a posteriori RB estimators, avoiding a discrete inf-sup lower bound estimate. We try to use less common ingredients of the RB framework to retrieve a better approximation of the RB error, such as the estimation of the distance between the continuous solution and the reduced one. In particular we focus on the application of the reduction model for the flow simulations in underground fractured media, in which high accurate simulations suffer for the complexity of the domain geometry. Finally, some numerical tests are assessed to confirm the viability and the efficacy of the technique proposed.

Keywords: Discrete Fracture Network flow simulations, Reduced Basis Method, Simulations in complex geometries, Mesh adaptivity, A posteriori error estimates, Adaptivity

1. Introduction

Given a partial differential equation (PDE) dependent from a set of parameters, the Reduced Basis Method (RBM) is a well known and valid technique to generate a numerical solution dependent on a set of parameters from a linear combination of a small group of detailed high fidelity solutions, each one simulated from a selected parameter value. The selection of this special sub-set of solutions is usually performed resorting to an error analysis on a larger training set of solutions, called "snapshots". According

to [1, 2, 3], standard techniques for RB offline greedy error analysis relies on the quality of the high fidelity solutions, thus snapshots should be very accurate; moreover, the RB a posteriori error estimators strongly depend on the value of the condition number of the matrix of the high fidelity problem. Some problems in modern applied engineering, such as the simulation of underground phenomena in fractured media, hardly satisfy the properties required by classical RB a posteriori estimators. Fracture network geometries are usually generated from random probability distributions yielding to strong geometrical complexities on the domains. This results in hard difficulties in conforming mesh generation, that is sometime infeasible or yields to a huge number of unknowns to fit the geometrical constraints, also where the solution does not display significant behaviours. A variety of strategies are proposed in literature to overcome these problems, such as [4, 5, 6] in which little geometry modifications are performed, or such as [7, 8, 9, 10] in which the authors try to relax or remove the conformity constraints on fracture intersections. In the present work we focus on a PDE-constrained optimization method applied to Discrete Fracture Networks (DFN), introduced in [11] and validated in [12], to avoid the geometrical complexities in the generation of the mesh on the fracture intersections and to remarkably reduce the number of unknowns of the discrete problem. We show that classic RBM error estimators are not effective to the fracture network problem when using non-conforming meshes due to the small value of the inf-sup constant of the discretized problem [13]. Moreover, we try to propose an alternative RBM greedy offline error estimator to build a reliable RB space thanks to a residual-based a posteriori error estimate available in [14] and [15] associated to the optimization method. Section 2 introduces the greedy approach proposed. In Section 3 we report the DFN variational parametrized PDE problem. Finally, Section 4 introduces the reduction applied to the DFN discrete problem and the greedy a posteriori analysis. The error estimations is validated with some numerical tests in Section 5.

2. RB Error Estimates

The definition of a RB a posteriori error estimators is fundamental for the reliability of the RB method, see for example [1, 2, 16]. Given a set of parameters $\mu = (\mu_1, \ldots, \mu_{\mathcal{P}}) \in \mathcal{P} \subset \mathbb{R}^{\mathcal{P}}$ and two Hilbert spaces $\mathcal{X}$ and $\mathcal{Y}$ on $\mathbb{R}$ along with their dual $\mathcal{X}^*$ and $\mathcal{Y}^*$, we consider a parametrized variational numerical problem $P : \mathcal{P} \times D \to \mathcal{X}$ on the domain $D \subset \mathbb{R}^d$

$$a(w, v; \mu) = f(v; \mu) \quad \forall v \in \mathcal{Y}, \tag{1}$$

with $a(\cdot, \cdot; \mu) : \mathcal{X} \times \mathcal{Y} \to \mathbb{R}$ bilinear form and $f(\cdot; \mu) \in \mathcal{Y}^*$ bounded linear functional on $\mathcal{Y}$ for each $\mu \in \mathcal{P}$. We denote by $(\cdot, \cdot)_{\mathcal{X}}$ the inner product over the space $\mathcal{X}$ and by $\|\cdot\|_{\mathcal{X}}^2 = (\cdot, \cdot)_{\mathcal{X}}$ the induced norm. Moreover, $_{\mathcal{Y}^*}\langle f, v \rangle_{\mathcal{Y}}$ denotes the duality pairing between $\mathcal{Y}^*$ and $\mathcal{Y}$. In what follows we assume the well-posedness of the problem (1) with unique solution $w(\mu) \in \mathcal{X}$ for all $\mu \in \mathcal{P}$. For the Nečas theorem, this is equivalent [17] to guarantee the existence of a finite continuity upper bound constant $\gamma_{UB} > 0$ s.t. $\gamma(\mu) = \sup_{w \in \mathcal{X}} \sup_{v \in \mathcal{Y}} \frac{a(w,v;\mu)}{\|w\|_{\mathcal{X}} \|v\|_{\mathcal{Y}}} \leq \gamma_{UB}$, the inf-sup condition $\inf_{v \in \mathcal{Y}} \sup_{w \in \mathcal{X}} \frac{a(w,v;\mu)}{\|w\|_{\mathcal{X}} \|v\|_{\mathcal{Y}}} > 0$

and a finite inf-sup lower bound constant $\beta_{LB} > 0$ s.t.

$$\beta(\mu) = \inf_{w \in \mathcal{X}} \sup_{v \in \mathcal{Y}} \frac{a(w, v; \mu)}{\|w\|_{\mathcal{X}} \|v\|_{\mathcal{Y}}} \geq \beta_{LB}. \tag{2}$$

Under these assumptions, choosing $\mathcal{X}_\delta \subset \mathcal{X}$ and $\mathcal{Y}_\delta \subset \mathcal{Y}$ as closed subspaces of finite dimension δ, we approximate the continuos problem (1) with the following weak discrete problem $P_\delta : \mathscr{P} \times D \to \mathcal{X}_\delta$

$$a(w_\delta, v; \mu) = f(v; \mu) \quad \forall v \in \mathcal{Y}_\delta. \tag{3}$$

Let $w_\delta(\mu) \in \mathcal{X}_\delta$ be the unique solution of problem (3) and $w_N(\mu) \in \mathcal{X}_N \subseteq \mathcal{X}_\delta$ the solution of the reduced problem $P_N : \mathscr{P} \times D \to \mathcal{X}_N$

$$a_N(w_N, v; \mu) = f_N(v; \mu) \quad \forall v \in \mathcal{Y}_N, \tag{4}$$

being $\mathcal{X}_N \subset \mathcal{X}_\delta$ and $\mathcal{Y}_N \subset \mathcal{Y}_\delta$ subspaces of dimension N. Classical a posteriori RB estimators have the goal to approximate for each $\mu \in \mathscr{P}$ the norm of the error $\mathrm{e}_{\delta,N}$: $\mathcal{X}_\delta \times \mathcal{X}_N \to \mathcal{X}_\delta$ s.t.

$$\mathrm{e}_{\delta,N}(w_\delta, w_N; \mu) := w_\delta(\mu) - \mathbb{V}w_N(\mu), \tag{5}$$

being $\mathbb{V} \in \mathbb{R}^{\delta \times N}$ the column-wise collection of the orthonormal basis $\{\zeta_n\}_{n \in \{1, \dots, N\}}$ of $\mathcal{X}_N$. Assuming the well-posedness of problem (3) for each $\mu \in \mathscr{P}$ there exists a discrete inf-sup lower bound $\beta_{\delta,LB} > 0$ s.t.

$$\beta_\delta(\mu) = \inf_{w \in \mathcal{X}_\delta} \sup_{v \in \mathcal{Y}_\delta} \frac{a(w, v; \mu)}{\|w\|_{\mathcal{X}} \|v\|_{\mathcal{Y}}} \geq \beta_{\delta,LB}. \tag{6}$$

Following [17], classical RB theory introduces a posteriori estimator $\Delta_N : \mathscr{P} \times \mathcal{X}_N \to \mathbb{R}$, defined $\forall \mu \in \mathscr{P}$ as

$$\Delta_N(w_N; \mu) := \frac{\left\| R_\delta(\mathbb{V}w_N; \mu) \right\|_{\mathcal{Y}^*}}{\beta_\delta(\mu)}, \tag{7}$$

where we indicate with $R_\delta : \mathscr{P} \times \mathcal{X}_\delta \to \mathbb{R} \in \mathcal{Y}_\delta^*$ the discrete residual $\forall v \in \mathcal{Y}_\delta$

$$_{\mathcal{Y}^*}\langle R_\delta(w_\delta; \mu), v \rangle_{\mathcal{Y}} := f(v; \mu) - a(w_\delta, v; \mu). \tag{8}$$

For the sake of notational simplicity, $\Delta_N(w_N; \mu)$ and $\mathrm{e}_{\delta,N}(w_\delta, w_N; \mu)$ will be shortened to $\Delta_N(\cdot; \mu)$ and $\mathrm{e}_{\delta,N}(\cdot; \mu)$. In order to evaluate the reliability of (7) we introduce the effectivity index $\eta_N(\mu) := \frac{\Delta_N(\cdot; \mu)}{\|\mathrm{e}_{\delta,N}(\cdot; \mu)\|_{\mathcal{X}}}$. Using the discrete continuity constant $\gamma_\delta(\mu)$, from classical theory follows

$$1 \leq \eta_N(\mu) \leq \frac{\gamma_\delta(\mu)}{\beta_\delta(\mu)} = \kappa_\delta(\mu), \tag{9}$$

being $\kappa_\delta(\mu)$ the condition number of the matrix associated to the high fidelity problem P_δ. The error estimation $\left\| \mathrm{e}_{\delta,N}(\cdot; \mu) \right\|_{\mathcal{X}} \leq \Delta_N(w_N; \mu)$ is the base for most of the RB greedy algorithms for the construction of the RB space $\mathcal{X}_N$, starting from a sufficiently large sample set $S_M = \{\mu^1, \dots, \mu^M\} \subseteq \mathscr{P}$.

3

Algorithm 1 reports the steps required to obtain matrix $\mathbb{V}$ we introduced in (5) for a given a tolerance $\varepsilon_N > 0$, see [1, 16, 17]. The quantity (7) is computed using

$$\Delta_{N,I}(w_N; \mu) := \frac{\left\| R_\delta(\mathbb{V} w_N; \mu) \right\|_{\mathcal{Y}^*}}{\beta_{\delta,I}(\mu)} \tag{10}$$

with the use of a suitable interpolatory approximation $\beta_{\delta,I} : \mathscr{P} \to \mathbb{R}$ in place of the exact value $\beta_\delta(\mu)$ for each $\mu \in \mathscr{P}$, [18]. Other reliable tecniques to approximate the inf-sup constants may be used, such as the SCM introduced in [19].

Algorithm 1 RB Greedy Space Basis Construction - Classic

Input: $\varepsilon_N > 0, S_M = \{\mu^1, \ldots, \mu^M\} \subseteq \mathscr{P}, \beta_{\delta,I} : \mathscr{P} \to \mathbb{R}$
Output: $N \geq 0, \mathbb{V} = [\zeta_1, \ldots, \zeta_N] \in \mathbb{R}^{\delta \times N}$
  1: Initialize $\mathbb{V} = [], N = 0, \delta_N = \varepsilon_N + 1, \mu_s^1 = \text{rand}(S_M)$
  2: **while** $N < M \wedge \delta_N > \varepsilon_N$ **do**
  3:      $N = N + 1$
  4:      Compute $w_\delta(\mu_s^N)$ solving P_δ
  5:      $\zeta_N = \text{GramSchmidt}(\mathbb{V}, w_\delta(\mu_s^N))$
  6:      $\mathbb{V} = [\mathbb{V}, \zeta_N]$
  7:      Compute $\mathbb{S}_{N,M} = [w_N(\mu^1), \ldots, w_N(\mu^M)] \in \mathbb{R}^{N \times M}$ solving P_N
  8:      $\mu_s^{N+1} = \arg \max_{\mu \in S_M} \Delta_{N,I}(w_N; \mu)$
  9:      $\delta_N = \Delta_{N,I}(w_N; \mu_s^{N+1}) / \left\| w_N(\mu_s^{N+1}) \right\|_{\mathcal{X}}$
 10: **end while**

Our target is to provide an estimate of $e_{\delta,N}(\cdot; \mu)$ for problems P_δ in which the discrete inf-sup $\beta_\delta(\mu)$ is very small $\forall \mu \in \mathscr{P}$ and the condition number $\kappa_\delta(\mu)$ grows rapidly when the complexity of the problem increases. Other authors perform a similar task, such as the hierarchical methods introduced in [2]. However, in DFN flow simulation with no conformity requirements on the mesh at fracture intersections, accurate high-fidelity solutions w_δ are not easy to obtain, [13]. We introduce for all $\mu \in \mathscr{P}$ the quantities $e_N : \mathcal{X} \times \mathcal{X}_N \to \mathcal{X}$ and $e_\delta : \mathcal{X} \times \mathcal{X}_\delta \to \mathcal{X}$ defined by

$$e_N(w, w_N; \mu) := w(\mu) - \mathbb{V} w_N(\mu), \quad e_\delta(w, w_\delta; \mu) := w(\mu) - w_\delta(\mu), \tag{11}$$

suitable to measure the distances between the solution of the continuous problem $w(\mu)$ from the reduced one $w_N(\mu)$ and from the discrete one $w_\delta(\mu)$. As we did for (5), $e_N(w, w_N; \mu)$ and $e_\delta(w, w_\delta; \mu)$ in (11) will be shorten to $e_N(\cdot; \mu)$ and $e_\delta(\cdot; \mu)$. In [20] and [3], the same quantities are already investigated for similar purposes. Assuming the mesh for the high fidelity problem fixes, for each parameter $\mu \in \mathscr{P}$ we consider the triangle formed by $w(\mu), w_\delta(\mu)$ and $w_N(\mu)$. From Figure 1, we can note that when $\left\| e_{\delta,N}(\cdot; \mu) \right\|_{\mathcal{X}} \to 0$

$$\left\| e_{\delta,N}(\cdot; \mu) \right\|_{\mathcal{X}} \approx \left| \| e_\delta(\cdot; \mu) \|_{\mathcal{X}} - \| e_N(\cdot; \mu) \|_{\mathcal{X}} \right|, \tag{12}$$

thanks to the cosine rule. Based on this relation, we introduce a new algorithm to build the RB space which takes in account the distance between the exact solution $w(\mu)$ and
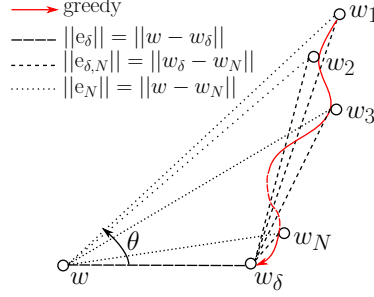
Figure 1: Algorithm 2 - Intuitive explanation

the reduced solution $w_N(\mu)$. The residual based a posteriori error estimate [21] ensures the existence of two positive constants $C^* > 0$ and $C_* > 0$ independent of the mesh size s.t.

$$C_* \Delta_\delta(w_\delta; \mu) \leq \|e_\delta(w, w_\delta; \mu)\|_\chi \leq C^* \Delta_\delta(w_\delta; \mu), \tag{13}$$

where $\Delta_\delta : \mathscr{P} \times \mathcal{X}_\delta \to \mathbb{R}$ is a discrete residual-based a posteriori error estimator, [15, 22]. Let us define $\Delta_{\delta,N} : \mathscr{P} \times \mathcal{X}_N \to \mathbb{R}$ for each $\mu \in \mathscr{P}$ as

$$\Delta_{\delta,N}(w_N; \mu) := \Delta_\delta(\mathbb{V} w_N; \mu). \tag{14}$$

The error in (12) can be estimated by

$$\left| \|e_\delta(\cdot; \mu)\|_\chi - \|e_N(\cdot; \mu)\|_\chi \right| \approx \left| \Delta_\delta(w_\delta; \mu) - \Delta_{\delta,N}(w_N; \mu) \right|, \tag{15}$$

thanks to $\mathcal{X}_N \subseteq \mathcal{X}_\delta$ and to the Petrov-Galerkin orthogonality which holds for (3) and (4), as shown in [17]. $\Delta_\delta(w_\delta; \mu)$ and $\Delta_{\delta,N}(w_N; \mu)$ will be shortened to $\Delta_\delta(\cdot; \mu)$ and $\Delta_{\delta,N}(\cdot; \mu)$ in next sections. In estimation (15) we do not include the constants C_* and C^* because we assume them uniformly bounded with respect to the parameter μ, [22]. Finally, similar to the approach provided in (10), we introduce a suitable interpola-

---

Algorithm 2 Greedy RB Space Basis Construction - Exact Solution

---

Input: $\varepsilon_N > 0$, $S_M = \{\mu^1, \ldots, \mu^M\} \subseteq \mathscr{P}$, $\Delta_{\delta,I} : \mathscr{P} \to \mathbb{R}$
Output: $N \geq 0$, $\mathbb{V} = [\zeta_1, \ldots, \zeta_N] \in \mathbb{R}^{\delta \times N}$
 1: Initialize $\mathbb{V} = []$, $N = 0$, $\delta_N = \varepsilon_N + 1$, $\mu_s^1 = \text{rand}(S_M)$
 2: **while** $N < M \wedge \delta_N > \max\{\varepsilon_N, \varepsilon_\delta\}$ **do**
 3:     $N = N + 1$
 4:     Compute $w_\delta(\mu_s^N)$ solving P_δ
 5:     $\zeta_N = \text{GramSchmidt}(\mathbb{V}, w_\delta(\mu_s^N))$
 6:     $\mathbb{V} = [\mathbb{V}, \zeta_N]$
 7:     Compute $\mathbb{S}_{N,M} = [w_N(\mu^1), \ldots, w_N(\mu^M)] \in \mathbb{R}^{N \times M}$ solving P_N
 8:     $\mu_s^{N+1} = \arg\max_{\mu \in S_M} \left| \Delta_{\delta,N}(w_N; \mu_s^{N+1}) - \Delta_{\delta,I}(\mu_s^{N+1}) \right|$
 9:     $\delta_N = \left| \Delta_{\delta,N}(w_N; \mu_s^{N+1}) - \Delta_{\delta,I}(\mu_s^{N+1}) \right| / \Delta_{\delta,I}(\mu_s^{N+1})$
10: **end while**

---

tion $\Delta_{\delta,I} : \mathscr{P} \to \mathbb{R}$ in place of the estimator value $\Delta_\delta(\cdot; \mu)$ for each $\mu \in \mathscr{P}$. Then,

104 Algorithm 2 provides the reduced space basis using (15) to capture the maximum vari-
105 ability of the error avoiding the dependency from the discrete inf-sup constant $\beta_\delta(\mu)$.
106 Moreover, referring again to Figure 1 and using the triangle inequality

$$\|e_N(\cdot;\mu)\|_\chi \le \|e_\delta(\cdot;\mu)\|_\chi + \left\|e_{\delta,N}(\cdot;\mu)\right\|_\chi \le (\varepsilon_\delta + \varepsilon_N) \|w_\delta(\cdot;\mu)\|_\chi \tag{16}$$

107 we can choose the tolerance of the RB method ε_N in the same order of magnitude of
108 the tolerance to control the high fidelity error ε_δ, to obtain an RBM error proportional
109 to the discrete one.

3. DFN Model

111 In what follows we provide a brief description of the DFN model, which represents
112 a network of geological fractures on an impervious rock matrix, [15, 23, 24, 25, 22].
113 The discrete network

$$\mathcal{F} := \bigcup_{i \in \mathcal{I}} F_i \subseteq D \subset \mathbb{R}^3 \tag{17}$$

114 collects all the fractures F_i, $i \in \mathcal{I} = \{1, \dots, I\}$, represented as planar polygons in the
115 three dimensional domain $D \subset \mathbb{R}^3$. The set of segments collecting all the intersections
116 between two fractures is denoted by $\mathcal{S} := \bigcup_{m \in \mathcal{M}} S^m$ with $S^m := \bar{F}_i \cap \bar{F}_j$, $m \in \mathcal{M} =$
117 $\{1, \dots, M\}$; fracture intersections are addressed as "traces" below. A bijective map
118 $I_S : \mathcal{M} \mapsto \mathcal{I} \times \mathcal{I}$ is directly defined by $I_S(m) = (i, j)$ with $i < j$. As a natural extension
119 of the notation introduced, $\mathcal{S}_i = \mathcal{S}|_{F_i}$ will denote the subset of traces restricted to F_i
120 and $\mathcal{M}_i$ their trace's indices. The network boundary $\partial \mathcal{F}$ is split in the Dirichlet part
121 Γ_D, with $|\Gamma_D| > 0$ and the Neumann part $\Gamma_N = \partial \mathcal{F} \setminus \Gamma_D$; $b^D \in H^{\frac{1}{2}}(\Gamma_D)$ is imposed
122 on Γ_D and an homogeneous Neumann conditions is imposed on Γ_N; see [23] for more
123 details on non homogeneous Neumann boundary conditions. Finally, on the restricted
124 sets $\Gamma_{iD} = \Gamma_D|_{F_i}$ the intuitive $b_i^D := b^D|_{\Gamma_{iD}}$ boundary functions are imposed.

3.1. The Continuos Problem

126 Out target is the computation of the hydraulic head H ruled by a Darcy's law on the
127 full network $\mathcal{F}$. For each $i \in \mathcal{I}$, let us introduce the functional spaces $V_i^D := H_D^1(F_i) =$
128 $\{v \in H^1(F_i) : v|_{\Gamma_{iD}} = b_i^D\}$, $V_i := H_0^1(F_i) = \{v \in H^1(F_i) : v|_{\Gamma_{iD}} = 0\}$ and the problem
129 $H_i \in V_i^D$ s.t. $\forall v \in V_i$

$$\int_{F_i} K_i \nabla H_i \nabla v \, dF = \int_{F_i} Q_i v \, dF + \sum_{m=1}^M \int_{S^m} \left[\!\left[\frac{\partial H_i}{\partial \hat{v}_i^m} \right]\!\right] v|_{S^m} \, d\gamma. \tag{18}$$

130 K_i represents the fracture hydraulic conductivity tensor that here is assumed to be con-
131 stant on the fracture F_i, Q_i the source term of the fracture and $\left[\!\left[\frac{\partial H_i}{\partial \hat{v}_i^m} \right]\!\right]$ the jump of the co-
132 normal derivative of the hydraulic head along the unit vector $\hat{v}_i^m$ of F_i on each $S^m \in \mathcal{S}_i$
133 with $\frac{\partial H_i}{\partial \hat{v}_i^m} = K_i \nabla H_i \cdot \hat{v}_i^m$. Finally, two conditions on each $S^m \in \mathcal{S}$ shall be imposed to

guarantee the continuity of the hydraulic head on the intersections and the balance of the normal fluxes; thus, for all $m \in \mathcal{M}$

$$H_i|_{S^m} - H_j|_{S^m} = 0, \tag{19}$$

$$\left[\!\!\left[\frac{\partial H_i}{\partial \hat{v}_i^m}\right]\!\!\right] + \left[\!\!\left[\frac{\partial H_j}{\partial \hat{v}_j^m}\right]\!\!\right] = 0, \tag{20}$$

with i and j induced by the map $I_S(m)$.

The introduced model can be converted into an equivalent optimization problem, see [11, 15] for further details, introducing the spaces $V := \prod_{i \in \mathcal{I}} V_i^D$, $W_m := \mathrm{H}^{-\frac{1}{2}}(S^m)$ and $W_m^* := \mathrm{H}^{\frac{1}{2}}(S^m) \; \forall m \in \mathcal{M}$ and the quantity $U_m^i \in W_m$

$$U_m^i := \left[\!\!\left[\frac{\partial H_i}{\partial \hat{v}_i^m}\right]\!\!\right] + \alpha H_i|_{S^m}, \tag{21}$$

with $\alpha > 0$ an arbitrary positive constant introduced for the well posedness of the flow problem on each F_i. Conditions (19) and (20) can be replaced by the minimization of the functional $J : V \times W \to \mathbb{R}$

$$J(H, U) = \sum_{m=1}^{M} \left\|H_i|_{S^m} - H_j|_{S^m}\right\|_{W_m^*}^2 + \left\|U_i^m + U_j^m - \alpha\left(H_i|_{S^m} + H_j|_{S^m}\right)\right\|_{W_m}^2 \tag{22}$$

for all $H \in V$ and being $U \in W := \prod_{m \in \mathcal{M}}(W_m \times W_m)$. Introducing the following bilinear forms $a_{F_i} : V_i^D \times V_i \to \mathbb{R}$ and $a_{S_i} : W_m \times W_m^* \to \mathbb{R}$

$$a_{F_i}(u, v) := (\nabla u, \nabla v)_{\mathrm{L}^2(F_i)}, \quad a_{S_i}(q, s) := \sum_{S^m \in \mathcal{S}_i} {}_{W_m^*}\langle s, q \rangle_{W_m}. \tag{23}$$

Darcy's equation (18) can be shortened applying the constraint functional $G_i : V_i^D \times W_m \times V_i \to \mathbb{R}$ defined as

$$G_i(H_i, U_i^m, v) = 0 \Leftrightarrow a_{F_i}(K_i H_i, v) + a_{S_i}(\alpha H_i|_{S^m} - U_i^m, v|_{S^m}) - (Q_i, v)_{\mathrm{L}^2(F_i)} = 0 \tag{24}$$

Thus, the set of equations (18)-(19)-(20) are equivalently replaced [11] by the optimization problem find $H \in V$ s.t.

$$\min_{U \in W} J(H, U) \text{ s.t. } G_i(H_i, U_i^m, v) = 0 \quad \forall i \in \mathcal{I}, \tag{25}$$

with U the control variable of the problem given by the cartesian product of U_i^m for all $S^m \in \mathcal{S}_i$ with $i \in \mathcal{I}$. It is possible to reformulate the optimization problem (25), [15, 22], introducing a Lagrange multiplier $P \in V$, the space $\mathcal{X} := V \times W \times V$ and the space $\mathcal{Y} := V \times W^* \times V$. A Lagrangian functional $\mathscr{L} : \mathcal{X} \times \mathcal{Y} \to \mathbb{R}$ can be defined for $w := (H, U, P) \in \mathcal{X}$, $r := (v, t, q) \in \mathcal{Y}$

$$\begin{aligned}
\mathscr{L}(w, r) := \sum_{i \in \mathcal{I}} &a_{F_i}(K_i H_i, v_i) + a_{S_i}(\alpha H_i|_{S^m} - U_i^m, v_i|_{S^m}) + \\
&a_{F_i}(K_i P_i, q_i) - a_{S_i}(H_i|_{S^m} - H_j|_{S^m}, q_i|_{S^m}) + \\
a_{S_i}(U_i^m + U_j^m - \alpha&\left(H_i|_{S^m} + H_j|_{S^m}\right) + P_i|_{S^m}, t|_{S^m}) - (Q_i, v_i)_{\mathrm{L}^2(F_i)},
\end{aligned} \tag{26}$$

7

154 where $P_i := P|_{F_i} \in V_i$, $v_i := v|_{F_i} \in V_i$ and $q_i := q|_{F_i} \in V_i$. By referring to [11], problem

$$\mathcal{L}(w, v) = 0, \quad \forall v \in \mathcal{Y} \tag{27}$$

155 has an unique solution $w := (H, U, P) \in \mathcal{X}$ equivalent to the one of the optimization
156 problem (25) and, thanks to the Nečas theorem, it is possible to prove the inf-sup
157 condition (2) with the space norm $\|\cdot\|_{\mathcal{X}}$ defined as follows: given $w := (H, U, P) \in \mathcal{X}$

$$\|w\|_{\mathcal{X}}^2 := \sum_{i \in \mathcal{I}} K_i |H_i|_{H^1(F_i)}^2 + K_i |P_i|_{H^1(F_i)}^2 +$$
$$\sum_{S^m \in \mathcal{S}_i} \left(\|\alpha H_i|_{S^m}\|_{L^2(S^m)}^2 + \|\alpha P_i|_{S^m}\|_{L^2(S^m)}^2 + \|U_i^m\|_{H^{-1/2}(S^m)}^2 \right), \tag{28}$$

158 with $|\cdot|_{H^1(F_i)}$ representing the semi-norm in the space $H^1(F_i)$.

159 ### 3.2. The Discrete Problem

160   Following the approach introduced in [25], the discretization of the problem is
161 performed independently on each fracture creating an independent mesh $\mathcal{T}_i$ on F_i and a
162 mesh $\mathcal{T}_i^m$ on each trace S^m in F_i. On each F_i we introduce the finite-dimensional space
163 $V_{\delta,i} := \text{span}\{\varphi_{i,k}\}_{k \in \{1,...,N_i\}} \subset V_i$ of dimension N_i. The set of functions $\{\varphi_{i,\ell}^D\}_{\ell \in \{1,...,N_{i,D}\}}$ is
164 used to discretize the lifting function on the Dirichlet boundary and the space $V_{\delta,i}^D :=$
165 $V_{\delta,i} \times \text{span}\{\varphi_{i,\ell}^D\}_{\ell \in \{1,...,N_{i,D}\}}$ of dimension $N_i^D := N_i + N_{i,D}$ is introduced. In the following,
166 the contractions $\mathcal{N}_i := \{1,...,N_i\}$, $\mathcal{N}_{i,D} := \{N_i + 1,...,N_i^D\}$ and $\mathcal{N}_i^D := \{1,...,N_i^D\}$ are
167 used. Similarly, we define on each S^m of F_i the finite-dimensional subspace $W_{\delta,i}^m :=$
168 $\text{span}\{\psi_{i,\ell}^m\}_{\ell \in \{1,...,N_i^m\}} \subset L^2(S^m) \subset W_m$ of dimension N_i^m. For the sake of notation, in the
169 following we use the same symbol to denote both the discrete functions and the vectors
170 of its degree of freedom (DOFs); for example h_i will state both for the function $h_i \in V_{\delta,i}^D$
171 and the real vector $h_i \in \mathbb{R}^{N_i^D}$. Therefore, the discrete hydraulic head $h_i \in V_{\delta,i}^D$ and the
172 discrete control variable $u_i^m \in W_{\delta,i}^m$ are naturally defined. Finally, we define the discrete
173 hydraulic head of the network as $h := (h_1, \ldots, h_I) \in V_\delta := \prod_{i \in \mathcal{I}} V_{\delta,i}^D$ of dimension
174 $N_{\mathcal{F}} = \sum_{i \in \mathcal{I}} N_i^D$ and the discrete control variable of the network $u := (u^1, \ldots, u^M) \in$
175 $W_\delta := \prod_{m \in \mathcal{M}} (W_{\delta,i}^m \times W_{\delta,j}^m)$ of dimension $N^{\mathcal{S}} = \sum_{m \in \mathcal{M}} (N_i^m + N_j^m)$, having set $u^m =$
176 $(u_j^m, u_j^m) \in W_{\delta,i}^m \times W_{\delta,j}^m$, with i and j taken from the map $I_S(m)$. The discrete counterpart
177 of Darcy's equation in (25) can be deduced introducing the matrices $\mathbb{A}_{F_i}, \mathbb{A}_{F_i}^D \in \mathbb{R}^{N_i^D \times N_i^D}$
178 and $\mathbb{A}_{\mathcal{S}_i}, \mathbb{A}_{\mathcal{S}_i}^D \in \mathbb{R}^{N_i^D \times N_i^D}$ defined by

$$\mathbb{A}_{F_i}|_{k\ell} = \begin{cases} a_{F_i}(\varphi_{i,k}, \varphi_{i,\ell}) & k,\ell \in \mathcal{N}_i \\ 1 & k = \ell \in \mathcal{N}_{i,D} \\ 0 & otherwise \end{cases}, \mathbb{A}_{F_i}^D|_{k\ell} = \begin{cases} a_{F_i}(\varphi_{i,k}, \varphi_{i,\ell}^D) & k \in \mathcal{N}_i, \ell \in \mathcal{N}_{i,D} \\ -1 & k = \ell \in \mathcal{N}_{i,D} \\ 0 & otherwise \end{cases}$$

$$\mathbb{A}_{\mathcal{S}_i}|_{k\ell} = \begin{cases} a_{\mathcal{S}_i}(\varphi_{i,k}|_{S^m}, \varphi_{i,\ell}|_{S^m}) & k,\ell \in \mathcal{N}_i \\ 0 & otherwise \end{cases}, \mathbb{A}_{\mathcal{S}_i}^D|_{k\ell} = \begin{cases} a_{\mathcal{S}_i}(\varphi_{i,k}|_{S^m}, \varphi_{i,\ell}^D|_{S^m}) & k \in \mathcal{N}_i, \ell \in \mathcal{N}_{i,D} \\ 0 & otherwise \end{cases}. \tag{29}$$

179 The matrix $\mathcal{B}_i \in \mathbb{R}^{N_i^D \times N^{\mathcal{S}}}$ is also introduced to collect the integrals of the product of
180 basis functions $\{\varphi_{i,k}|_{S^m}\}_{k \in \{1,...,N_i^D\}}$ with $\{\psi_{i,\ell}^m\}_{\ell \in \{1,...,N_i^m\}}$ for all $S^m \in \mathcal{S}_i$. Therefore, for

each $i \in \mathcal{I}$ we obtain the discrete version of (24), $G_{\delta,i}(h, u) : V_\delta \times W_\delta \to \mathbb{R}$ with $G_{\delta,i}(h, u) := \mathbb{A}_i h_i - q_i + \mathbb{A}_i^D h_i^D - \mathcal{B}_i u$, with matrix $\mathbb{A}_i = K_i \mathbb{A}_{F_i} + \alpha \mathbb{A}_{\mathcal{S}_i} \in \mathbb{R}^{N_i^D \times N_i^D}$, matrix $\mathbb{A}_i^D = K_i \mathbb{A}_{F_i}^D + \alpha \mathbb{A}_{\mathcal{S}_i}^D \in \mathbb{R}^{N_i^D \times N_i^D}$, vector $q_i \in \mathbb{R}^{N_i^D}$ the discretization of the forcing term Q_i and vector $h_i^D \in \mathbb{R}^{N_i^D}$ the evaluation of the Dirichlet boundary conditions b_i^D. Finally, let us introduce the block-diagonal matrices $\mathbb{A} := \text{diag}(\mathbb{A}_i)_{i \in \mathcal{I}} \in \mathbb{R}^{N_\mathcal{F} \times N_\mathcal{F}}$ and $\mathbb{A}^D := \text{diag}(\mathbb{A}_i^D)_{i \in \mathcal{I}} \in \mathbb{R}^{N_\mathcal{F} \times N_\mathcal{F}}$, the column-wise collection matrix $\mathcal{B} := (\mathcal{B}_1, \ldots, \mathcal{B}_I) \in \mathbb{R}^{N_\mathcal{F} \times N^S}$ and the column vectors $q := (q_1, \ldots, q_I)$, $h^D := (h_1^D, \ldots, h_I^D) \in \mathbb{R}^{N_\mathcal{F}}$ to obtain the discrete constraints equation

$$\mathbb{A}h - q + \mathbb{A}^D h^D - \mathcal{B}u = 0, \tag{30}$$

simply denoted by $G_\delta(h, u) = 0$. In the discrete framework, the functional (22) can be written using $L^2(S^m)$ norms in place of W_m and W_m^* norms, obtaining the discrete functional $J_\delta : V_\delta \times W_\delta \to \mathbb{R}$

$$J_\delta(h, u) := \frac{1}{2} \left(h^T \mathbb{G}^h h - \alpha h^T \mathbb{B}^h u - \alpha u^T \mathbb{B}^u h + u^T \mathbb{G}^u u \right). \tag{31}$$

The matrix $\mathbb{B}^h = (\mathbb{B}^u)^T \in \mathbb{R}^{N_\mathcal{F} \times N^S}$ collects the integrals of the mixed products between basis functions of V_δ and W_δ and the matrix $\mathbb{G}^u \in \mathbb{R}^{N^S \times N^S}$ is the mass matrix of the products between the traces basis functions. Furthermore, the matrix $\mathbb{G}^h \in \mathbb{R}^{N_\mathcal{F} \times N_\mathcal{F}}$ is defined as the sum $\mathbb{G}^h = (\alpha^2 + 1)\mathbb{G}_\mathcal{F}^h + (\alpha^2 - 1)\mathbb{G}_\mathcal{S}^h$, with $\mathbb{G}_\mathcal{F}^h \in \mathbb{R}^{N_\mathcal{F} \times N_\mathcal{F}}$ column-wise combination $\forall S^m \in \mathcal{S}_i$ of matrices $\mathbb{G}_{F_i}^h \in \mathbb{R}^{N_i^D \times N_\mathcal{F}}$

$$(\mathbb{G}_{F_i}^h)_{k\hat{\ell}(i)} = (\varphi_{i,k}^\star|_{S^m}, \varphi_{i,\ell}^\star|_{S^m}) \quad k, \ell \in \mathcal{N}_i^D, \tag{32}$$

and $\mathbb{G}_\mathcal{S}^h \in \mathbb{R}^{N_\mathcal{F} \times N_\mathcal{F}}$ column-wise combination $\forall S^m \in \mathcal{S}_i$ of matrices $\mathbb{G}_{S^m}^h \in \mathbb{R}^{N_i^D \times N_\mathcal{F}}$

$$(\mathbb{G}_{S^m}^h)_{k\hat{\ell}(j)} = (\varphi_{i,k}^\star|_{S^m}, \varphi_{j,\ell}^\star|_{S^m}) \quad k \in \mathcal{N}_i^D, \ \ell \in \mathcal{N}_j^D, \tag{33}$$

with i and j taken from the map $I_S(m)$, $\hat{\ell}(i) = \sum_{p<i} N_p^D + \ell$ and the symbol $\star$ shall be left empty or shall substitute with D according to the indices numbering. Thus, the discrete counterpart of problem (25) becomes find $h \in V_\delta$

$$\min_{u \in W_\delta} J_\delta(h, u) \text{ s.t. } G_\delta(h, u) = 0. \tag{34}$$

Following the same approach applied for the definition of (26), this optimization discrete problem can be solved introducing the adjoint Lagrange multiplier $p \in V_\delta$. Appling the Galerkin approach with the definition of the space $\mathcal{X}_\delta := V_\delta \times W_\delta \times V_\delta$, we obtain the discrete Lagrangian functional $\mathscr{L}_\delta : \mathcal{X}_\delta \to \mathbb{R}$ defined for all $w_\delta := (h, u, -p) \in \mathcal{X}_\delta$ as

$$\mathscr{L}_\delta(w_\delta) = J_\delta(h, u) - p^T G_\delta(h, u), \tag{35}$$

which leads to the following optimality system

$$\mathbb{M}_\delta w_\delta = f_\delta, \tag{36}$$

9

where

$$\mathbb{M}_\delta := \left(\begin{array}{ccc} \mathbb{G}^h & -\alpha\mathbb{B}^h & \mathbb{A}^T \\ -\alpha\mathbb{B}^u & \mathbb{G}^u & -\mathcal{B}^T \\ \mathbb{A} & -\mathcal{B} & 0 \end{array} \right), \quad f_\delta := \left(\begin{array}{c} 0 \\ 0 \\ q - \mathbb{A}^D h^D \end{array} \right),$$

with $\mathbb{M}_\delta \in \mathbb{R}^{(2N_\mathcal{F}+N^\mathcal{S}) \times (2N_\mathcal{F}+N^\mathcal{S})}$ and $f_\delta \in \mathbb{R}^{2N_\mathcal{F}+N^\mathcal{S}}$. The matrix $\mathbb{M}_\delta$ is symmetric and non singular, [26], and the solution of the equation (36) is the unique minimizer of (34). Due to the choice of not conformity meshes on the traces, taking a trace mesh coarser with respect to the fracture mesh, we have a non vanishing discrete inf-sup lower bound $\beta_{\delta,LB}$, with possible very small values, [13]. Thus, classical RBM a posteriori theory can be unreliable as it is well outlined in next section.

3.3. The Parametrized Problem

The optimization problem (34) and the linear system (36) are now rewritten as a parametrized problem dependent from a set of parameters $\mu = (\mu_1, \ldots, \mu_\mathcal{P}) \in \mathscr{P} \subset \mathbb{R}^\mathcal{P}$

$$\min_{u \in W_\delta} \ J_\delta(h, u; \mu) \ \text{s.t.} \ G_\delta(h, u; \mu) = 0, \tag{37}$$

$$\mathbb{M}_\delta(\mu) w_\delta(\mu) = f_\delta(\mu). \tag{38}$$

The set of parameters $\mathscr{P}$ is chosen following the model we apply to compute K_i on each fracture F_i. A common approach used in the applications, [27], is to define a three-dimensional stochastic field $\mathcal{K} : D \times \Omega \to \mathbb{R}$ and the distribution of $K_i(\omega)$ is computed as the mean value $K_i(\omega) := \frac{1}{|F_i|} \int_{F_i} \mathcal{K}(x, \omega) \, dx$. According to geological measurements, $\mathcal{K}(x, \omega)$ may follows the law $\mathcal{K}(x, \omega) = b^{L(x,\omega)}$, where $b > 1$ is a constant and $L : D \times \Omega \to \mathbb{R}$ is a stochastic field with measurable mean value $\mathbb{E}[L] : D \to \mathbb{R}$ and covariance function $C_L : D \times D \to \mathbb{R}$. Assuming C_L continuos on its domain, the Karhunen-Loève decomposition of L can be applied, see [28, 29], as follows $L(x, \omega) = \mathbb{E}[L](x) + \sum_{n=1}^\infty \sqrt{\lambda_n} \varphi_n(x) Y_n(\omega)$, where (λ_n, φ_n) is the eigenvalue-eigenvector pair of the compact operator $T\varphi = \int_D C_L(z, \cdot) \varphi(z) \, dz$ and Y_n are mutually uncorrelated random variables with $\mathbb{E}[Y_n] = 0$ and $\mathbb{E}[Y_n^2] = 1$. As in [29], we consider $C_L(x, z) = \exp\left(-\frac{\|x-z\|_2^2}{\gamma^2}\right)$, being γ the measure of the correlation length and Y_n uniformly distributed; hence $Y_n \sim \mathcal{U}(-\sqrt{3}, \sqrt{3}) = \sqrt{3}(2\tilde{Y}_n - 1)$, with $\tilde{Y}_n \sim \mathcal{U}(0, 1)$. Finally, we define $\mathscr{P} := \prod_{p=1}^\mathcal{P} [0, 1] \subset \mathbb{R}^\mathcal{P}$ and we truncate the K.-L. series to the sum of $\mathcal{P}$ terms obtaining $L_\mathcal{P} : D \times \mathscr{P} \to \mathbb{R}$ defined as $L_\mathcal{P}(x; \mu) := \mathbb{E}[L](x) + \sum_{p=1}^\mathcal{P} \sqrt{\lambda_p} \varphi_p(x) \mu^p$.

Therefore, we introduce $\mathcal{K}_\mathcal{P}(x; \mu) = b^{L_\mathcal{P}(x;\mu)} : D \times \mathscr{P} \to \mathbb{R}$ and for each $i \in \mathcal{I}$ the conductivity parameter map $K_{i,\mathcal{P}} : \mathscr{P} \to \mathbb{R}$ becomes

$$K_{i,\mathcal{P}}(\mu) := \frac{1}{|F_i|} \int_{F_i} \mathcal{K}_\mathcal{P}(x; \mu) \, dx. \tag{39}$$

This definition allows us to show the μ-affine, or μ-separable form of the parametric linear system (38): replacing the constant α introduced in (21) with a positive parametric

function $\alpha : \mathscr{P} \to \mathbb{R}^+$ chosen arbitrarily, we have for each $\mu \in \mathscr{P}$

$$
\mathbb{M}_\delta(\mu) = \mathbb{M}_\delta^c + \alpha(\mu)\mathbb{M}_\delta^{\mathcal{S}} + (\alpha^2(\mu) + 1)\mathbb{M}_\delta^{\mathbb{G}_{\mathcal{F}}^h} + (\alpha^2(\mu) - 1)\mathbb{M}_\delta^{\mathbb{G}_{\mathcal{S}}^h} + \sum_{i \in \mathcal{I}} K_{i,\mathscr{P}}(\mu)\mathbb{M}_\delta^{\mathcal{F},i},
$$
$$
f_\delta(\mu) = f_\delta^c - \alpha(\mu)f_\delta^{\mathcal{S}} - \sum_{i \in \mathcal{I}} K_{i,\mathscr{P}}(\mu)f_\delta^{\mathcal{F},i}.
\tag{40}
$$

The following matrices in $\mathbb{R}^{(2N_{\mathcal{F}}+N^{\mathcal{S}})\times(2N_{\mathcal{F}}+N^{\mathcal{S}})}$ are defined as

$$
\mathbb{M}_\delta^c := \begin{pmatrix} 0 & 0 & 0 \\ 0 & \mathbb{G}^u & -\mathcal{B}^T \\ 0 & -\mathcal{B} & 0 \end{pmatrix}, \mathbb{M}_\delta^{\mathcal{F},i} := \begin{pmatrix} 0 & 0 & \mathbb{A}_{\mathcal{F},i}^T \\ 0 & 0 & 0 \\ \mathbb{A}_{\mathcal{F},i} & 0 & 0 \end{pmatrix}
$$

$$
\mathbb{M}_\delta^{\mathcal{S}} := \begin{pmatrix} 0 & -\mathbb{B}^h & \mathbb{A}_{\mathcal{S}}^T \\ -\mathbb{B}^u & 0 & 0 \\ \mathbb{A}_{\mathcal{S}} & 0 & 0 \end{pmatrix}, \mathbb{M}_\delta^{\mathbb{G}_{\mathcal{F}}^h} := \begin{pmatrix} \mathbb{G}_{\mathcal{F}}^h & 0 & 0 \\ 0 & 0 & 0 \\ 0 & 0 & 0 \end{pmatrix}, \mathbb{M}_\delta^{\mathbb{G}_{\mathcal{S}}^h} := \begin{pmatrix} \mathbb{G}_{\mathcal{S}}^h & 0 & 0 \\ 0 & 0 & 0 \\ 0 & 0 & 0 \end{pmatrix}
$$

and the right-hand-side vectors in $\mathbb{R}^{(2N_{\mathcal{F}}+N^{\mathcal{S}})}$ are defined as $f_\delta^c := (0,0,q)^T$, $f_\delta^{\mathcal{S}} :=$ $(0,0,\mathbb{A}_{\mathcal{S}}^D h^D)^T$ and $f_\delta^{\mathcal{F},i} := (0,0,\mathbb{A}_{\mathcal{F},i}^D)^T$. Block-diagonal matrices $\mathbb{A}_{\mathcal{S}} := \mathrm{diag}(\mathbb{A}_{\mathcal{S}_i})_{i \in \mathcal{I}} \in$ $\mathbb{R}^{N_{\mathcal{F}}\times N_{\mathcal{F}}}$ and $\mathbb{A}_{\mathcal{S}}^D := \mathrm{diag}(\mathbb{A}_{\mathcal{S}_i}^D)_{i \in \mathcal{I}} \in \mathbb{R}^{N_{\mathcal{F}}\times N_{\mathcal{F}}}$ are defined applying (29); similarly, matrices $\mathbb{A}_{\mathcal{F},i} \in \mathbb{R}^{N_{\mathcal{F}}\times N_{\mathcal{F}}}$ and $\mathbb{A}_{\mathcal{F},i}^D \in \mathbb{R}^{N_{\mathcal{F}}\times N_{\mathcal{F}}}$ are created as follow for each $i \in \mathcal{I}$

$$
\mathbb{A}_{\mathcal{F},i}^\star := \begin{pmatrix} 0 & \dots & 0 \\ \vdots & \mathbb{A}_{F_i}^\star & \vdots \\ 0 & \dots & 0 \end{pmatrix},
\tag{41}
$$

in which the symbol $\star$ shall be left empty or shall substitute with D according to the matrix to define. The matrices $\mathbb{G}^u$, $\mathbb{G}_{\mathcal{F}}^h$, $\mathbb{G}_{\mathcal{S}}^h$, $\mathcal{B}$, $\mathbb{B}^h$ are defined in (31)-(33). Equation (40) is usually written in the classical affine compact form

$$
\sum_{q=1}^{Q_{\mathbb{M}}} \theta_{\mathbb{M}}^q(\mu)\mathbb{M}_\delta^q w_\delta(\mu) = \sum_{q=1}^{Q_f} \theta_f^q(\mu)f_\delta^q,
\tag{42}
$$

where $Q_{\mathbb{M}} = I + 4$, $Q_f = I + 2$ and $\theta_{\mathbb{M}}^q$, $\theta_f^q : \mathscr{P} \to \mathbb{R}$ are μ-dependent functions.

4. The Reduction Strategy

For the reduction of problem (37) we consider an aggregated trial space strategy to guarantee the stability of the reduced approximation, [17, 30, 31, 1]. As before, we use the same symbol to denote both the discrete functions and the vectors of its DOFs. Choosing $N_\mu \in \mathbb{R}$, we define for each $\mu^n \in \mathscr{P}$, $n \in (1,\dots,N_\mu)$ the spaces $V_{N_{h,p}} :=$ $\mathrm{span}\{h(\mu^n), p(\mu^n)\} \subset V_\delta$ and $W_{N_u} := \mathrm{span}\{u(\mu^n)\} \subset W_\delta$ of dimension $N_{h,p} = 2N_\mu$ and $N_u = N_\mu$ respectively. Space $V_{N_{h,p}}$ represents the "aggregated" space for the state and adjoint variables, introduced to recover the inf-sup condition of the reduced problem (4) required for the stability of the RB approximation, [31].

11

The reduction of equation (38) can be performed introducing the space $\mathcal{X}_N := V_{N_{h,p}} \times W_{N_u} \times V_{N_{h,p}} \subset \mathcal{X}_\delta$ of dimension $N = 2N_{h,p} + N_u$ and the matrix

$$\mathbb{V} := diag(\mathbb{V}_{h,p}, \mathbb{W}_u, \mathbb{V}_{h,p}) \in \mathbb{R}^{(2N_{\mathcal{F}}+N^S)\times N},$$

with $\mathbb{V}_{h,p} \in \mathbb{R}^{N_{\mathcal{F}} \times N_{h,p}}$ the column-wise collection of $\{\zeta_n\}_{n \in \{1,\ldots,N_{h,p}\}}$ orthonormal basis of $V_{N_{h,p}}$ and $\mathbb{W}_u \in \mathbb{R}^{N^S \times N_u}$ the column-wise collection of $\{\xi_n\}_{n \in \{1,\ldots,N_u\}}$ orthonormal basis of W_{N_u}. Calling $w_N := (h_N, u_N, p_N) \in \mathcal{X}_N$ we obtain the reduced problem

$$\mathbb{V}^T \mathbb{M}_\delta(\mu) \mathbb{V} w_N(\mu) = \mathbb{V}^T f_\delta(\mu) \Leftrightarrow \mathbb{M}_N(\mu) w_N(\mu) = f_N(\mu) \tag{43}$$

in which we apply the Galerkin-RB approximation hypothesis, see [17] for further details. In conclusion, having defined a classical RB projection base on space $\mathcal{X}_N$, the whole RB methodology is available, such as POD or greedy algorithms for the selection of the RB-basis $\mathbb{V}$. Moreover, the affine parametric dependence of the operators, proved in (42), allows us to use the offline / online decomposition in order to obtain the solution of the problem.

4.1. DFN Error Estimates

We introduce the matrix $\mathbb{X}_\delta \in \mathbb{R}^{(2N_{\mathcal{F}}+N^S)\times(2N_{\mathcal{F}}+N^S)}$ to compute, given $w_\delta = (h, u, p) \in \mathcal{X}_\delta$ the norm

$$\begin{aligned}
\|w_\delta\|_{\mathbb{X}_\delta}^2 := w_\delta^T \mathbb{X}_\delta w_\delta = \sum_{i \in \mathcal{I}} |h_i|_{\mathrm{H}^1(F_i)}^2 + |p_i|_{\mathrm{H}^1(F_i)}^2 + \\
\sum_{S^m \in \mathcal{S}_i} \left(\|h_i|_{S^m}\|_{\mathrm{L}^2(S^m)}^2 + \|p_i|_{S^m}\|_{\mathrm{L}^2(S^m)}^2 + \left\| u_i^m \right\|_{\mathrm{H}^{-1/2}(S^m)}^2 \right)
\end{aligned} \tag{44}$$

in which $\|\cdot\|_{\mathrm{H}^{-1/2}(S^m)} : W_{\delta,i}^m \to \mathbb{R}$ is approximated by $\left\| u_i^m \right\|_{\mathrm{H}^{-1/2}(S^m)}^2 = \sum_{\lambda \in \mathcal{T}_i^m} |\lambda| \left\| u_i^m \right\|_{\mathrm{L}^2(\lambda)}^2$, with λ the element of the mesh $\mathcal{T}_i^m$ chosen on S^m in F_i. Recalling $K_{i,\mathcal{P}}$ in definition (39) and choosing $\alpha^2(\mu) = \overline{K_{i,\mathcal{P}}(\mu)} = I^{-1} \sum_{i \in \mathcal{I}} K_{i,\mathcal{P}}$ in (28), it is possible to show that $\|w_\delta\|_{\mathcal{X}_\delta} \approx \alpha(\mu) \|\hat{w}_\delta\|_{\mathbb{X}_\delta}$, being $\hat{w}_\delta = (h, \alpha(\mu)^{-1}u, p)$. The residual R_δ introduced in (8) becomes for the DFN optimization problem $R_\delta(w_\delta; \mu) = \mathbb{M}_\delta(\mu) w_\delta(\mu) - f_\delta(\mu)$ and the the inf-sup constant $\beta_\delta(\mu)$ defined in (6) is computed in the discrete optimization problem (37) as the smallest singular value $\sigma_{\min}(\mathbb{X}_\delta^{-\frac{1}{2}} \mathbb{M}_\delta(\mu) \mathbb{X}_\delta^{\frac{1}{2}})$. Finally, we introduce the a posteriori error estimator $\Delta_\delta(\cdot; \mu)$ involved in (13) for problem (37) as in [15]. Let T and e the elements and the edges of mesh $\mathcal{T}_i$ on fracture F_i, $\eta_{H,i}^2 := \sum_T \frac{|T|^2}{K_{i,\mathcal{P}}} \left\| q_i + K_{i,\mathcal{P}} \Delta h_i \right\|_{\mathrm{L}^2(T)}^2$ the residual estimator of the Darcy's equation and $\eta_{P,i}^2 := \sum_T K_{i,\mathcal{P}} |p_i|_{\mathrm{H}^1(T)}^2$ the estimator of the discontinuity of h between the fractures. Moreover, we introduce $\xi_{U,i}^2 := \sum_e \frac{|e|}{K_{i,\mathcal{P}}} \left\| \left[\!\left[\frac{\partial h_i}{\partial \hat{\gamma}_i^m} \right]\!\right] - \tilde{u}_i \right\|_{\mathrm{L}^2(e)}^2$ the estimator for the approximation of the flux through the edges of the mesh, where $\tilde{u}_i := u_i^m - \alpha h_i|_{S^m}$ is non-zero only on $e \cap S^m \neq \emptyset$, $\forall S^m \in \mathcal{S}_i$. Similarly, being $\mathcal{T}_i^m$ the mesh of elements λ on each trace $S^m \in \mathcal{S}_i$, we denote by $\xi_{NC,m}^2 := \sum_\lambda \frac{|\lambda|}{K_{i,\mathcal{P}}} \left\| u_i^m - \alpha h_i|_{S^m} \right\|_{\mathrm{L}^2(\lambda)}^2$ the estimator for
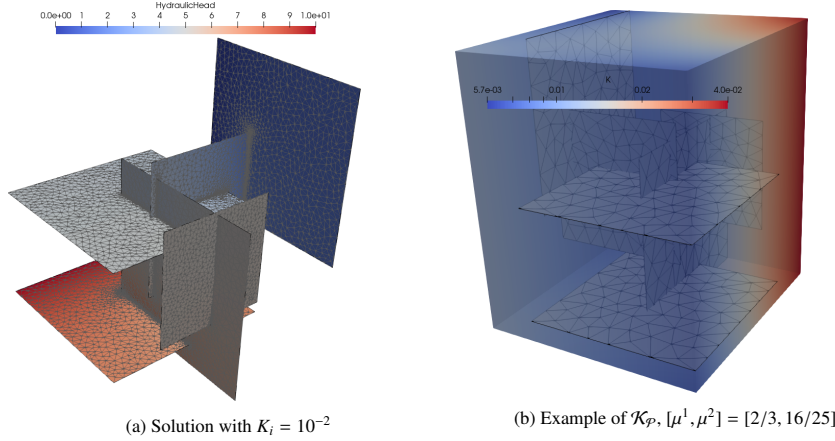
12

(a) Solution with $K_i = 10^{-2}$

(b) Example of $\mathcal{K}_\mathcal{P}$, $[\mu^1, \mu^2] = [2/3, 16/25]$

Figure 2: FracTest - Overview

(a) Problem size

ε_δ	$N_\mathcal{F}$	$N^\mathcal{S}$
10^{-1}	2,043	376
$5 \cdot 10^{-2}$	18,557	1,920

(b) Convergences Rates $\upsilon e^{-\rho N}$

Test	ε_δ	υ	ρ
$\Delta_{\delta,N}$	10^{-1}	$1.9133 \cdot 10^{-1}$	$1.2675 \cdot 10^{-1}$
Δ_N	10^{-1}	$1.3871 \cdot 10^{-1}$	$1.2847 \cdot 10^{-1}$
$\Delta_{\delta,N}$	$5 \cdot 10^{-2}$	$1.7179 \cdot 10^{-1}$	$1.1834 \cdot 10^{-1}$
Δ_N	$5 \cdot 10^{-2}$	$5.8893 \cdot 10^{-2}$	$1.1748 \cdot 10^{-1}$

Table 1: Frac6 - Data

the non-conformity of the discretization, by $\xi^2_{P,m} := \sum_\lambda \frac{|\lambda|}{K_{i,\mathcal{P}}} \|p_i|_{S^m}\|^2_{L^2(\lambda)}$ the estimator for the hydraulic head induced by the unbalancing of fluxes on the mesh and by $J^2_m :=$ $\sum_\lambda \frac{|\lambda|(1+\alpha)^2}{\min(K_{i,\mathcal{P}}, K_{j,\mathcal{P}})} \left\| u^m_i + u^m_j - \alpha(h_i|_{S^m} + h_j|_{S^m}) \right\|^2_{L^2(\lambda)} + \sum_\lambda \frac{|\lambda|}{\min(K_{i,\mathcal{P}}, K_{j,\mathcal{P}})} \left\| h_i|_{S^m} - h_j|_{S^m} \right\|^2_{L^2(\lambda)}$ the estimator of the functional minimization error. Collecting all the definitions the estimator turns out to be $\forall \mu \in \mathcal{P}$

$$\Delta^2_\delta(w_\delta; \mu) := \sum_{i \in \mathcal{I}} \left(\eta^2_{H,i} + \eta^2_{P,i} + \xi^2_{U,i} + \sum_{S^m \in \mathcal{S}_i} \left(\xi^2_{NC,m} + \xi^2_{P,m} + J^2_m \right) \right). \tag{45}$$

For the proof of (13) and further details of the definition of the quantities in (45) see [15, 22].

5. Numerical Results

For two different DFNs with growing complexity we perform the comparison of our estimator (Algorithm 2) with the classical greedy interpolation strategy proposed in [18] (Algorithm 1). Then, the RB certification is measured through the statistical

13

(a) $\Delta_\delta(\cdot;\mu)/\|w_\delta(\mu)\|_{\chi_\delta}$

(b) $\|w_\delta(\mu)\|_{\chi_\delta}$

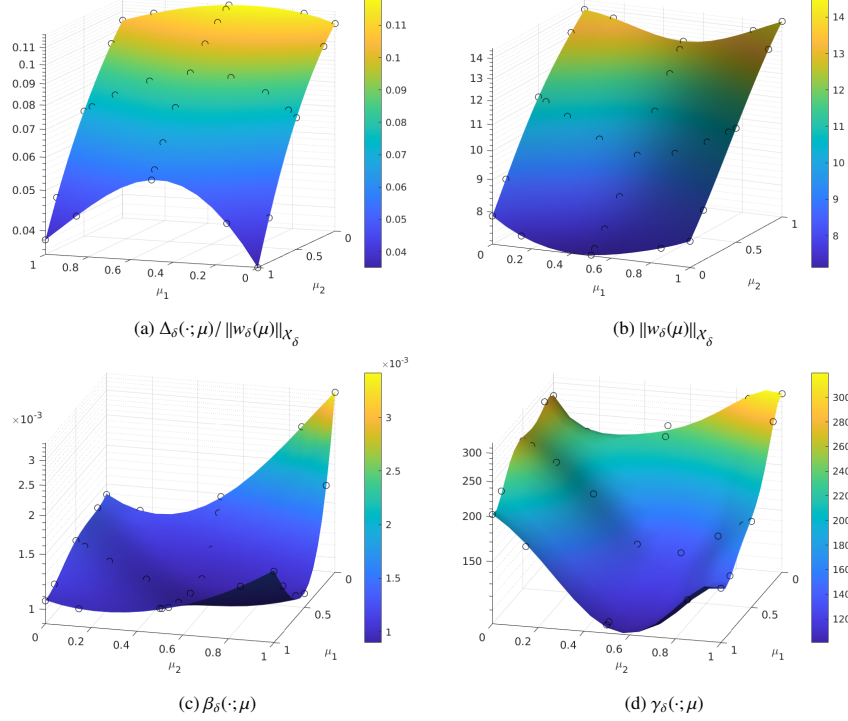(c) $\beta_\delta(\cdot;\mu)$

(d) $\gamma_\delta(\cdot;\mu)$

Figure 3: Frac6 - Interpolation with $\mathcal{P} = 2$, $I_\ell = 3$, $\varepsilon_\delta = 10^{-1}$. Black dots represent the sparse interpolation grid

analysis of the error $e_{\delta,N}$ on a random set of parameters $S_{\text{Test}} \subset \mathscr{P}$. The numerical tests are performed with relatively small DFNs because we focus on the validation of the proposed algorithm rather than on an efficient and robust implementation. The simulations for the resolution of the high-fidelity model are performed with the C++ software introduced in [12] applied to the optimization method of Section 3 and restricted to the serial case [32]. The post-processing analysis for the RBM theory provided in Section 4 is implemented in the MATLAB software.

5.1. Test 1 - DFN simple problem

The first test is performed on a simple problem called *Frac6*, with $I = 6$ and $M = 6$. Figure 2a shows the geometry of the network and an example of the solution of the discrete problem (37) computed with $K_i = 10^{-2}$ for all $i \in \mathcal{I}$ on an adaptive mesh. Two Dirichlet boundary conditions are imposed, namely a value of 10 in the bottom left fracture and a value of zero on the top right fracture; zero Neumann boundary conditions are required on the other borders and no forcing term is applied on each fracture. Figure 2b shows an example of the conductivity field $\mathcal{K}_\mathcal{P}$ with the DFN immersed; both the example and the following numerical tests are performed using $\mathscr{P}$ of dimension $\mathcal{P} = 2$ and taking the parameters of Conductivity field described in Section 4

14

equal to $\gamma = 0.25$, $\mathbb{E}[L] = -2$ and $b = 10$, that can be realistic values as already stated in [29]. The two meshes used to solve the high fidelity problem are choosen by the adaptive method described in [22] and are kept fixed independent of the dimension N of the space $\mathcal{X}_N$. The adapted meshes are obtained solving the optimization problem with parameter $K_i = b^{\mathbb{E}[L]} = 10^{-2} \; \forall i \in \mathcal{I}$, performing few adaptive iterations starting from a mesh with 100 DOFs and imposing two different values of the tolerance ε_δ (16) equal to 10^{-1} and 10^{-2}. Table 1a shows the resulting size of the discrete problem in both the tests. Figures 3 and 4 show the interpolation of all the quantities used in the RBM offline computations in both the tests; the surfaces are generated starting from a Smolyak's sparse grid [33] of level $I_\ell = 3$, to mitigate the curse of dimensionality problem with higher $\mathcal{P}$. A radial basis functions (RBF) interpolations of degree 5 of the relative a posteriori error $\Delta_\delta(\cdot; \mu)/ \|w_\delta(\mu)\|_{\mathcal{X}_\delta}$ and of the norm $\|w_\delta(\mu)\|_{\mathcal{X}_\delta}$ are represented in Figures 3a-4a and in Figures 3b-4b. Finally, the discrete inf-sup constant $\beta_\delta(\cdot; \mu)$ and the discrete continuity constant $\gamma_\delta(\cdot; \mu)$ are approximated with a least squares approximation of degree 5 and reported in Figures 3c-3d and Figures 4c-4d. The computation of the $\beta_\delta(\cdot; \mu)$ and $\gamma_\delta(\cdot; \mu)$ values in the interpolation points are performed as described in Section 4.1. Comparing Figure 3c and Figure 4c we can notice that the shape of the surfaces seems not to be influenced by the mesh size. Moreover, recalling (9), we can see that the effectivity index $\eta_\delta(\cdot; \mu)$ on the domain $\mathcal{P}$ in both cases is bounded by an average condition number $\kappa_\delta(\cdot; \mu)$ in the order of 10^5; this means that, even in this small and simple DFN, the classic RBM estimation $\Delta_N(\cdot, \mu)$ can be quite inaccurate. Figure 6 shows the convergences of both the greedy Algorithms 1 and 2 in which we impose $\varepsilon_N = 10^{-8}$ and $M = 100$. Although not required, in Algorithm 2, we compute also the classical RBM estimator $\Delta_N(\cdot; \mu)$ for comparison reasons. Figure 5a shows the set S_M used as input of both the algorithms and generated by a classic uniform tensorial $\mathcal{P}$-grid generated from a 1D-Chebyshev grid of size 10. Focusing on the convergence obtained, by comparing Figure 6a and Figure 6b we can say again that the mesh size does not have relevant impacts on the convergence rate of the RB error $e_{\delta,N}(\cdot; \mu)$ in both the greedy algorithms. Moreover, the curves $\max_{\mu \in S_M} \Delta_N / \|w_N\|_{\mathcal{X}_\delta}$ in Figure 6 obtained by the two algorithms are almost overlapped, but the error estimator $\left| \Delta_{\delta,N} - \Delta_{\delta,I} \right| / \Delta_{\delta,I}$ seems not strongly influenced by the high condition number $\kappa_\delta(\cdot; \mu)$. Therefore, the two algorithms are performing the choice of the reduced basis in a similar way, but Algorithm 2 relies on a more sharp stopping criterion. As suggested in Section 2 from the triangle inequality (16), we set $\varepsilon_N \lesssim \varepsilon_\delta$ in order to stop the greedy Algorithm 2 as soon as possible without any loss of accurancy. In particular, the first test with $\varepsilon_N \lesssim \varepsilon_\delta = 10^{-1}$ comes to a good approximation with N between 10 and 20 and the second case with $\varepsilon_N \lesssim \varepsilon_\delta = 10^{-2}$ seems have an optimal stop at N between 20 and 40. In Figure 7 we report the dimension N for different ε_N reached by Algorithm 1 and Algorithm 2 for the two considered values of ε_δ; the plots confirm the effectivenes of Algorithm 2.

To validate the results of the greedy algorithms, we use the RBM space $\mathcal{X}_N$ obtained to compare the online solution with the corresponding high fidelity solution on a trial set $S_{\text{Test}} \subseteq [0, 1]^2$ (see Figure 5b) of size $|S_{\text{Test}}| = 100$ randomly generated with uniform distribution. Figure 8 shows for each ε_δ the real relative RB error $\left\| e_{\delta,N} \right\|_{\mathcal{X}_\delta} / \|w_N\|_{\mathcal{X}_\delta}$ computed for each $\mu_{\text{Test}} \in S_{\text{Test}}$ on two N; we measure all the quantities used inside the

15

(a) $\Delta_\delta(\cdot;\mu)/\|w_\delta(\mu)\|_{\chi_\delta}$

(b) $\|w_\delta(\mu)\|_{\chi_\delta}$

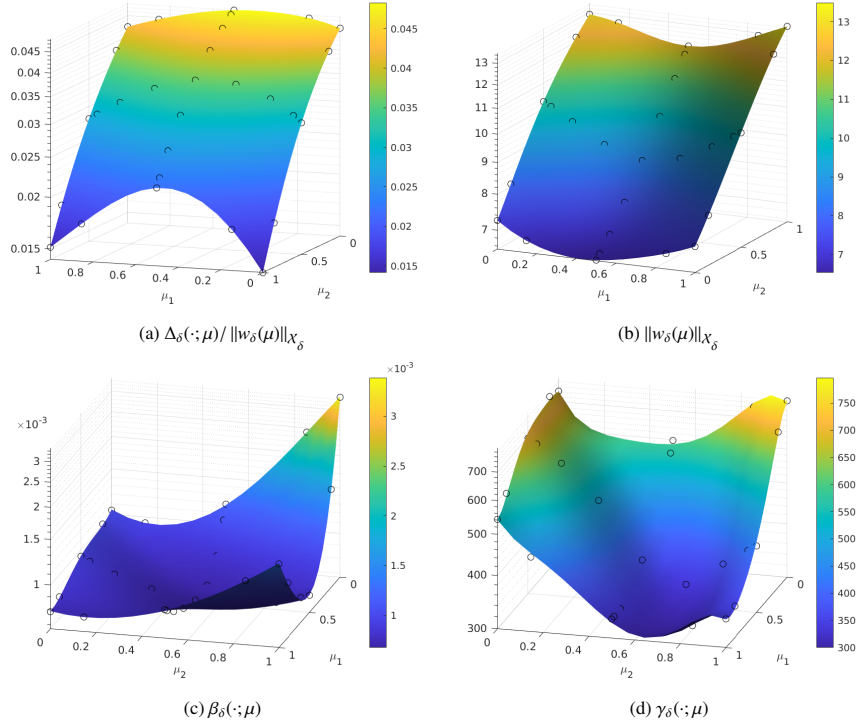(c) $\beta_\delta(\cdot;\mu)$

(d) $\gamma_\delta(\cdot;\mu)$

Figure 4: Frac6 - Interpolation with $\mathcal{P} = 2$, $I_\ell = 3$, $\varepsilon_\delta = 5\cdot10^{-2}$. Black dots represent the sparse interpolation grid
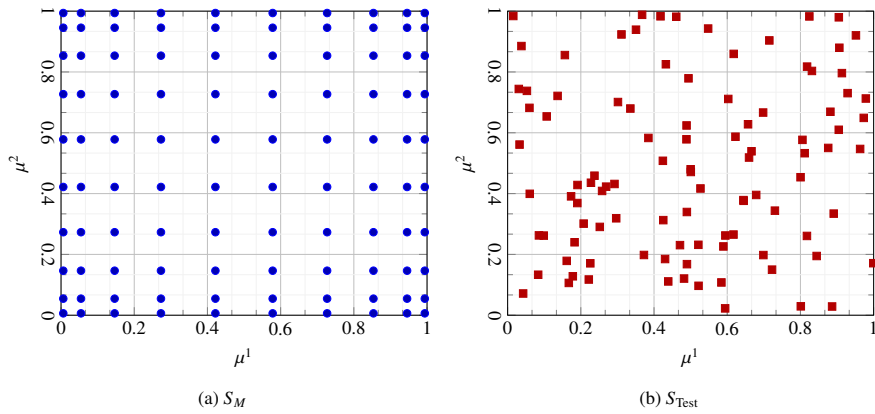

(a) S_M

(b) S_{Test}

Figure 5: Greedy Offline/Online set - $\mathscr{P}$ of dimension $\mathcal{P} = 2$

16

(a) $\varepsilon_\delta = 10^{-1}$

(b) $\varepsilon_\delta = 5 \cdot 10^{-2}$

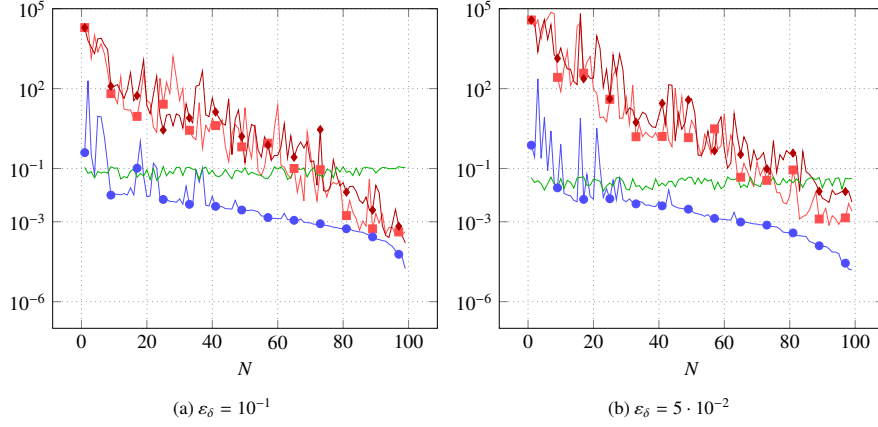Figure 6: Convergence of Algorithm 1 and Algorithm 2 applied to Frac6. Legend: ■— Algorithm 1 $\max_{\mu \in S_M} \Delta_N / \|w_N\|_{X_\delta}$, ◆— Algorithm 2 $\max_{\mu \in S_M} \Delta_N / \|w_N\|_{X_\delta}$, ●— $\max_{\mu \in S_M} |\Delta_{\delta,N} - \Delta_{\delta,I}| / \Delta_{\delta,I}$, —— $\max_{\mu \in S_M} \Delta_{\delta,I} / \|w_{\delta,I}\|_{X_\delta}$
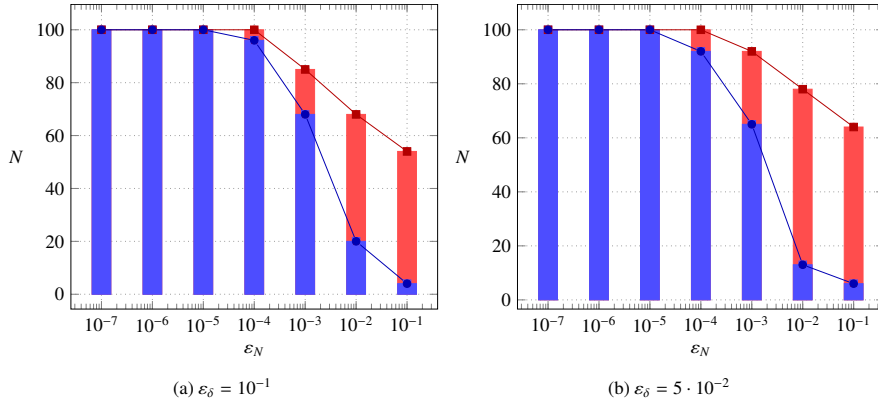

(a) $\varepsilon_\delta = 10^{-1}$

(b) $\varepsilon_\delta = 5 \cdot 10^{-2}$

Figure 7: Frac6 - Legend: ■— Convergence of Algorithm 1, ●— Convergence of Algorithm 2

17
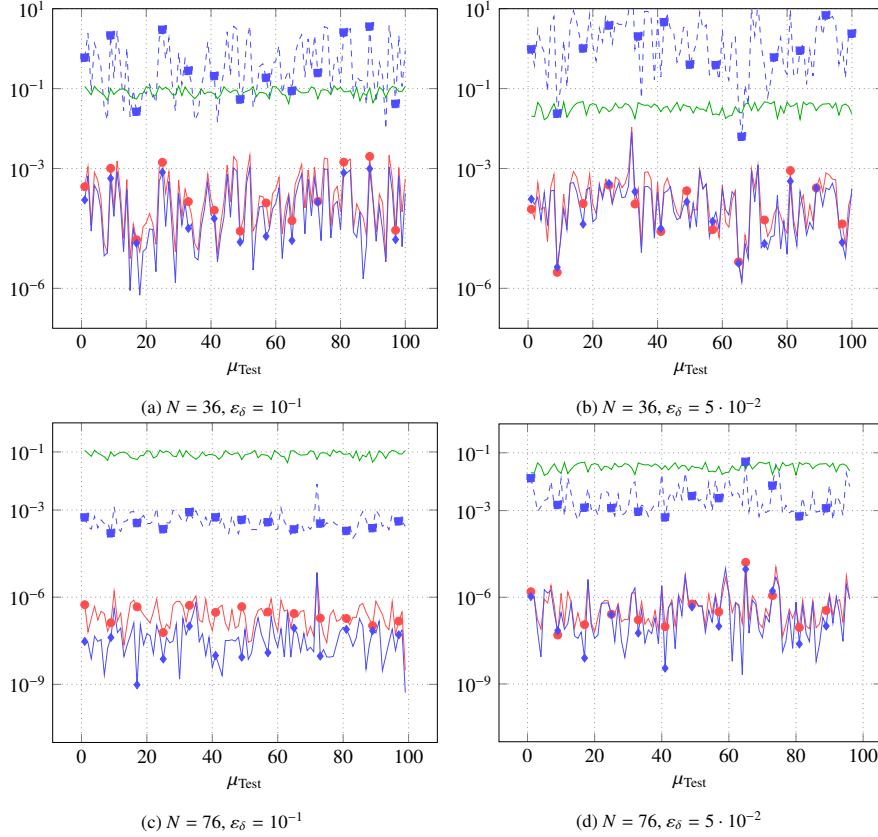
Figure 8: Frac6 - RBM Online, $|S_{\text{Test}}| = 100$. Legend: $- \blacksquare - \; \Delta_N / \|w_N\|_{\mathcal{X}_\delta}$, $\; \bullet \; \left\|e_{\delta,N}\right\|_{\mathcal{X}_\delta} / \|w_N\|_{\mathcal{X}_\delta}$, $\; \blacklozenge \;$ $\left|\Delta_{\delta,N} - \Delta_{\delta,I}\right| / \Delta_{\delta,I}$, $\; \underline{\hspace{1cm}} \; \Delta_{\delta,I} / \left\|w_{\delta,I}\right\|_{\mathcal{X}_\delta}$

greedy algorithms in order to compare the ability of the estimators to tackle the real error $e_{\delta,N}$. Relative estimator $\Delta_{\delta,I} / \left\|w_{\delta,I}\right\|_{\mathcal{X}_\delta}$ of error e_δ is also reported as a reference value for comparisons. As we expect, from the plots we can see that the relative classic RBM estimation $\Delta_N(\cdot; \mu)$ is far from the relative error even in this small case; on the other hand the new estimator proposed seems to be very close to the value expected. We shall remark that the estimator is not completely above or under the RBM error as we neglect the constants C_* and C^* in (15). From the very small distance between the curves we see in the plots, we can say that this assumption seems appropriate.

Figure 9 reports the average relative RBM error $\left\|e_{\delta,N}\right\|_{\mathcal{X}_\delta} / \|w_N\|_{\mathcal{X}_\delta}$ measured on the RBM online tests at different RB space size N, with its standard deviations; classic RBM estimator is also reported. Notice how the curve of the a posteriori error $\Delta_{\delta,I}$ related to the RB solution norm $\|w_N\|_{\mathcal{X}_\delta}$ becomes constant increasing N, thanks to the convergence of the RB solution to the discrete one w_δ. We can say that the results obtained on the trial set are compliant to the one depicted in Figure 7 in all the tests
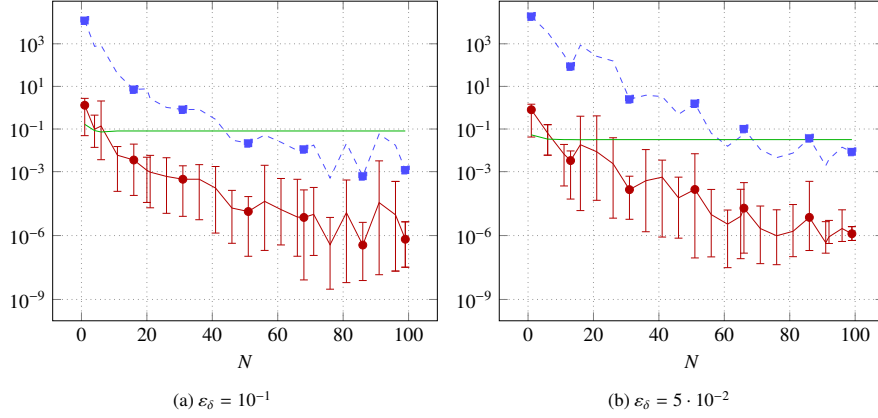
(a) $\varepsilon_\delta = 10^{-1}$ (b) $\varepsilon_\delta = 5 \cdot 10^{-2}$

Figure 9: Frac6 - RBM Online, $|S_{\text{Test}}| = 100$. Legend: ●— avg $\left\| e_{\delta,N} \right\|_{\mathcal{X}_\delta} / \|w_N\|_{\mathcal{X}_\delta}$, ■- avg $\Delta_N / \|w_N\|_{\mathcal{X}_\delta}$, —— avg $\Delta_{\delta,N} / \|w_N\|_{\mathcal{X}_\delta}$

performed. Moreover, the plots corroborate that no relevant differences can be observed comparing the corse mesh with respect to the finer one . To conclude the analysis, we report in Figure 10 and in Table 1b the convergence rates computed on the RBM error $\left\| e_{\delta,N} \right\|_{\mathcal{X}_\delta}$ obtained on the trial set S_{Test}; we remark that the symbol Δ_N identifies the estimator of Algorithm 1, whereas $\Delta_{\delta,N}$ identifies the estimator of Algorithm 2. We can see that an exponential convergence $\upsilon e^{-\rho N}$ typical of the Kolmogorov N-width decay of the elliptic equations is obtained also with the Algorithm 2. Finally, from Table 1b we can assert the rate of convergence ρ in the classical algorithm and in the new algorithm are comparable.

5.2. Test 2 - Real DFN

The second test is performed on an higher complexity stochastically generated DFN, called *Frac20*, with $I = 20$ and $M = 28$. The network is created with random probability distribution functions concerning size, position and orientation of fractures taken from the real data available in [34]. Even with a small number of fractures, in Figures 11a-11c we can appreciate the complexity of the geometry from three different point of view and an example of the solution of the discrete problem (37) computed through the model proposed with $K_i = 10^{-2}$ for all $i \in \mathcal{I}$. Focusing on Figure 11b, we impose a Dirichlet boundary condition of value 1 on the left side of the network and of value zero on the right part; always zero Neumann conditions are imposed on the other borders and no forcing term is present. As for the Frac6 test, Figure 11d shows a sample of the conductivity field $\mathcal{K}_\mathcal{P}$ with the DFN immersed; we keep the same parameter for the stochastic generation, therefore we use $\mathcal{P} = 2$, $\gamma = 0.25$, $\mathbb{E}[L] = -2$ and $b = 10$. We use a fixed adaptive mesh generated in the previous examples with $\varepsilon_\delta = 10^{-3}$ and Table 2a shows the resulting size of the discrete problem. From Figures 11 we can appreciate how the adaptive non-conforming method increases the number of mesh cells around the traces.
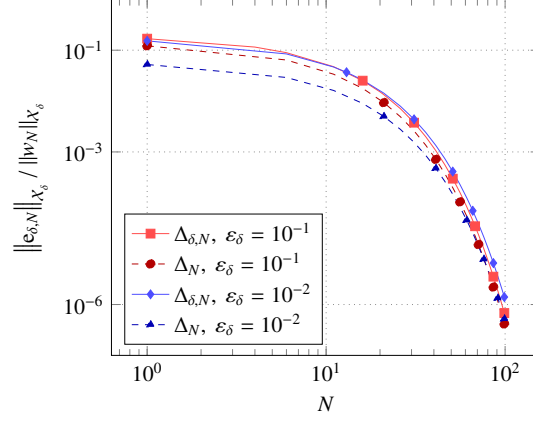
19

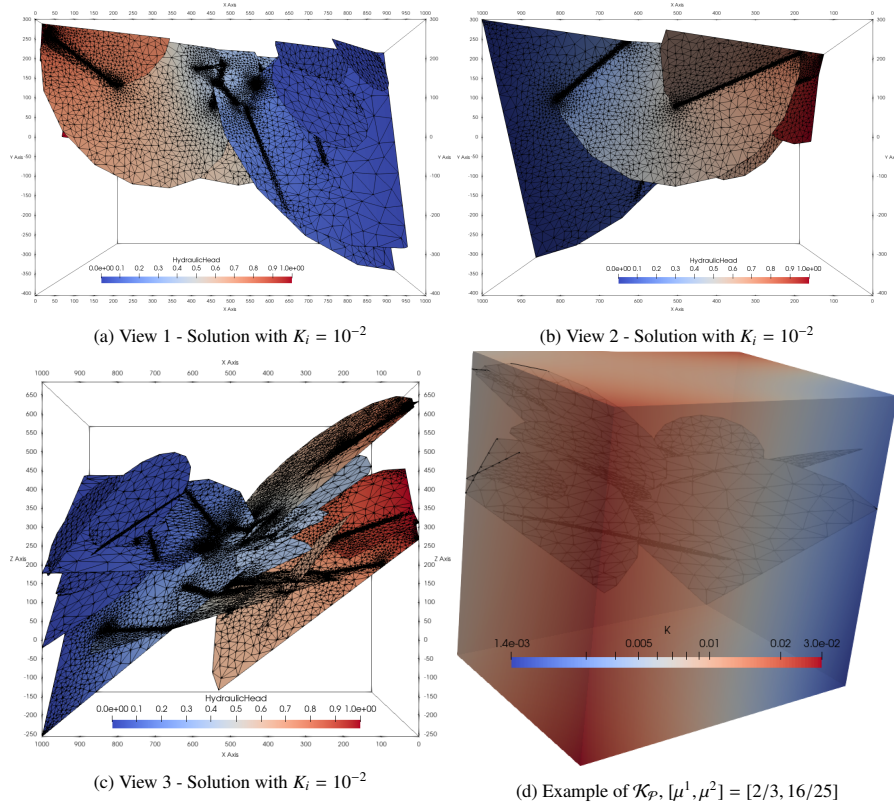Figure 10: Frac6 - Convergences Curves $\upsilon e^{-\rho N}$

(a) View 1 - Solution with $K_i = 10^{-2}$

(b) View 2 - Solution with $K_i = 10^{-2}$

(c) View 3 - Solution with $K_i = 10^{-2}$

(d) Example of $\mathcal{K}_{\mathcal{P}}$, $[\mu^1, \mu^2] = [2/3, 16/25]$

Figure 11: Frac20 - Overview

(a) $\Delta_\delta(\cdot;\mu)/\|w_\delta(\mu)\|_{\mathcal{X}_\delta}$

(b) $\|w_\delta(\mu)\|_{\mathcal{X}_\delta}$

(c) $\beta_\delta(\cdot;\mu)$
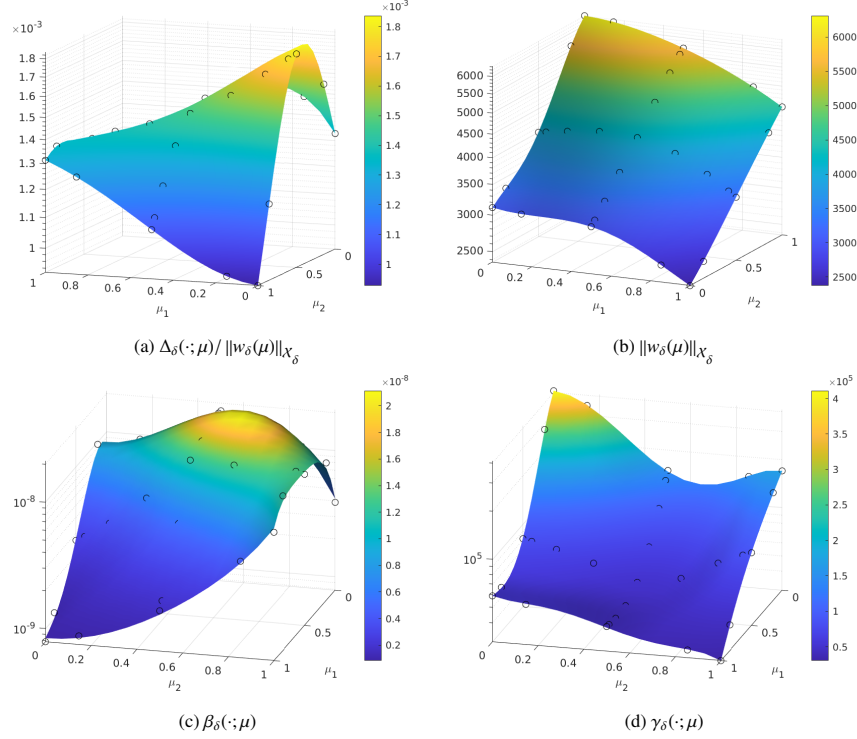
(d) $\gamma_\delta(\cdot;\mu)$

Figure 12: Frac20 - Interpolation with $\mathcal{P} = 2$, $I_\ell = 3$, $\varepsilon_\delta = 10^{-3}$. Black dots represent the sparse interpolation grid

Figure 12 shows the interpolation of all the quantities used in the RBM offline computations; again, a Smolyak's sparse grid quadrature rule of level $I_\ell = 3$ is used. RBF interpolation of degree 5 generates Figure 12a and Figure 12b; least squares approximation of degree 5 is used for Figure 12c and Figure 12d. Comparing Figures 12a-12d to Figures 3a-3d or to Figures 4a-4d it is possible to observe that each DFN has its own dependency from the parameter set $\mathcal{P}$. Moreover, recalling (9), we can see that the average $\kappa_\delta(\cdot;\mu)$ is above 10^{13}, therefore we expect the the classical RBM estimator Δ_N to be not reliable. Plots in Figure 13 shows the convergence of Algorithm 1 and Algorithm 2 obtained with $\varepsilon_N = 10^{-8}$ and $M = 100$. The classical RBM estimator $\Delta_N(\cdot;\mu)$ is reported for both the algorithms. As expected the classic RB estimator does not provide reliable information for stopping the iterations, on the other hand the new estimator seems to be effective. Moreover, Figure 13b clearly shows the effectivenes of Algorithm 2 to produce the RB space with a small value of N. In addition, in Figure 13a we observe a similar rate of convergence for the quantity $\Delta_N(\cdot;\mu)$. Taking $\varepsilon_N \lesssim \varepsilon_\delta = 10^{-3}$ to stop the greedy Algorithm 2 we can say that an acceptable convergence of the algorithm is performed with N between 60 and 80. To confirm these statements, we test the RBM space $\mathcal{X}_N$ obtained as done for the Frac6 test, evaluating the online solution on a trial set $S_{\text{Test}} \subseteq [0,1]^2$ of size $|S_{\text{Test}}| = 100$ randomly generated.
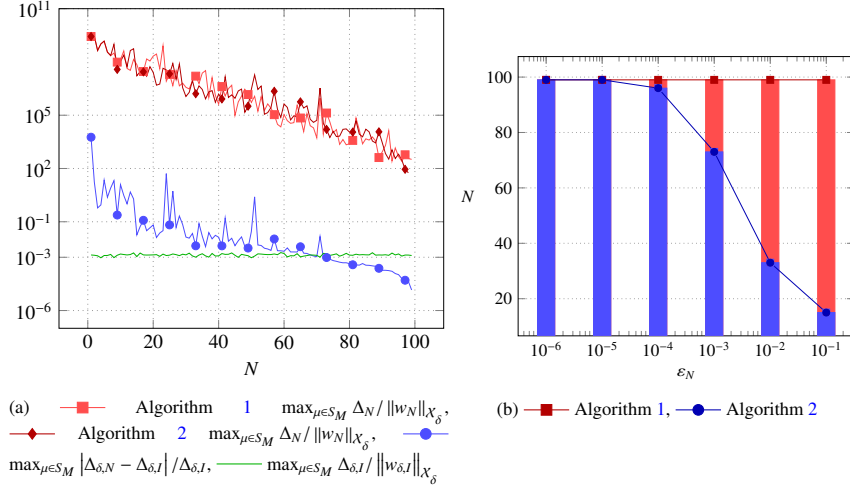
(a) ![legend] — Algorithm 1 $\max_{\mu \in S_M} \Delta_N / \|w_N\|_{\mathcal{X}_\delta}$,
— Algorithm 2 $\max_{\mu \in S_M} \Delta_N / \|w_N\|_{\mathcal{X}_\delta}$,
$\max_{\mu \in S_M} \left|\Delta_{\delta,N} - \Delta_{\delta,I}\right| / \Delta_{\delta,I}$, — $\max_{\mu \in S_M} \Delta_{\delta,I} / \|w_{\delta,I}\|_{\mathcal{X}_\delta}$

(b) — Algorithm 1, — Algorithm 2

Figure 13: Convergence of Algorithm 1 and Algorithm 2 applied to Frac20, $\varepsilon_\delta = 10^{-3}$

(a) Problem size

ε_δ	$N_{\mathcal{F}}$	$N^{\mathcal{S}}$
10^{-3}	25,880	2,922

(b) Convergences Rates $\upsilon e^{-\rho N}$

Test	ε_δ	υ	ρ
$\Delta_{\delta,N}$	10^{-3}	$1.4598 \cdot 10^2$	$1.1664 \cdot 10^{-1}$
Δ_N	10^{-3}	$1.4612 \cdot 10^2$	$1.1267 \cdot 10^{-1}$

Table 2: Frac20 - Data

Figure 14 displays all the quantities measured for each $\mu_{\text{Test}} \in S_{\text{Test}}$ on two N, including the real distance between the RBM solution and the discrete one $\left\|e_{\delta,N}\right\|_{\mathcal{X}_\delta} / \|w_N\|_{\mathcal{X}_\delta}$. The relative classic RBM $\Delta_N(\cdot; \mu)$ is far from the error, on the other hand the alternative estimator proposed is very close to the real error values. Again, the assumption to neglect the constants C_* and C^* is still reliable, as the estimator $\left|\Delta_{\delta,N} - \Delta_{\delta,I}\right| / \Delta_{\delta,I}$ is of the same size as the relative error $\left\|e_{\delta,N}\right\|_{\mathcal{X}_\delta} / \|w_N\|_{\mathcal{X}_\delta}$. To conclude the analysis, in Figure 15 we can see how the convergence rate of the average RB error $e_{\delta,N}(\cdot; \mu)$ measured matches with the values obtained in Figure 13b; again, the curve related to the DFN a posteriori estimator $\Delta_{\delta,N}(\cdot; \mu)$ becomes constant when N grows, thanks to the convergence of the RB solution w_N to the high fidelity one w_δ. Figure 15b and Table 2b confirm the exponential convergences $\upsilon e^{-\rho N}$ of the greedy method also with the stochastic DFN. We conclude the numerical tests reporting in Figure 16 two examples of the solution obtained with the RBM algorithm.

6. Conclusion

A simple and robust RBM greedy approach is proposed for the creation of a reduced basis space to approximate both the hydraulic head and the flux distribution on
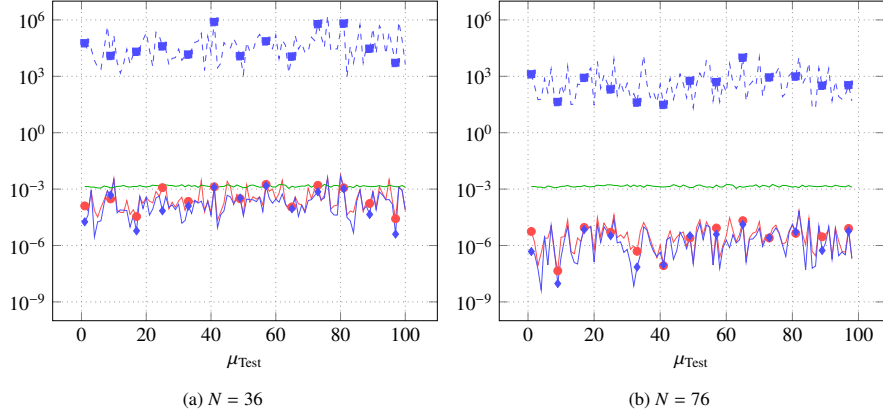
(a) $N = 36$

(b) $N = 76$

Figure 14: Frac20 - RBM Online, $|S_{\text{Test}}| = 100$, $\varepsilon_\delta = 10^{-3}$. Legend: $\Delta_N / \|w_N\|_{\mathcal{X}_\delta}$, $\left\|e_{\delta,N}\right\|_{\mathcal{X}_\delta} / \|w_N\|_{\mathcal{X}_\delta}$, $\left|\Delta_{\delta,N} - \Delta_{\delta,I}\right| / \Delta_{\delta,I}$, $\Delta_{\delta,I} / \left\|w_{\delta,I}\right\|_{\mathcal{X}_\delta}$

(a) $\left\|e_{\delta,N}\right\|_{\mathcal{X}_\delta} / \|w_N\|_{\mathcal{X}_\delta}$, $\Delta_N / \|w_N\|_{\mathcal{X}_\delta}$, $\Delta_{\delta,N} / \|w_N\|_{\mathcal{X}_\delta}$

(b) Convergences Curves $\upsilon e^{-\rho N}$
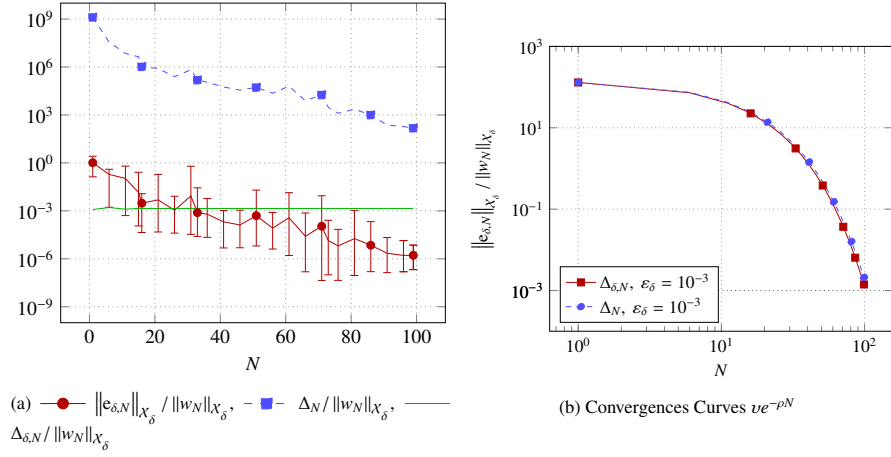
Figure 15: Frac20 - Test of RBM Online, $|S_{\text{Test}}| = 100$, $\varepsilon_\delta = 10^{-3}$

(a) $\mu = [0.080862; 0.77724]$

(b) $\mu = [0.74631; 0.010337]$
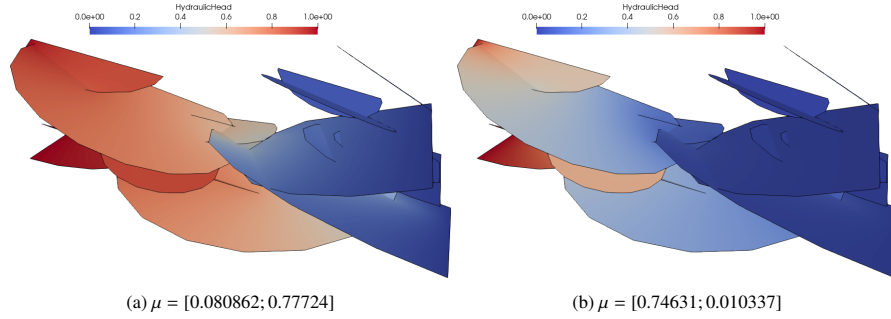
Figure 16: Frac20 - Solutions obtained with RBM

23

stochastic Discrete Fracture Networks. A smart stopping criterion for the greedy approach is also suggested to control the RBM space dimension taking the tolerance of the greedy algorithm in the same order of magnitude of the tolerance used for the a posteriori error estimate of the high fidelity solution. The algorithm relies on the a posteriori error estimation performed on the PDE-constrained optimization problem and it can be extended to a more fast and scalable solution by exploiting the parallel nature of non conforming mesh on each fracture of the network. Numerical tests verify the lower reliability of the classical RB a posteriori analysis and establish the validity of the alternative estimator showing the equivalence of the convergence rates compared to the classical RB methods.

References

[1] J. S. Hesthaven, G. Rozza, B. Stamm, Certified Reduced Basis Methods for Parametrized Partial Differential Equations, Springer, 2016.

[2] S. Hain, M. Ohlberger, Radic, K. Urban, A hierarchical a posteriori error estimator for the reduced basis method, Advances in Computational Mathematics 45 (5) (2019) 1572–9044.

[3] M. Ali, K. Steih, K. Urban, Reduced basis methods with adaptive snapshot computations, Advances in Computational Mathematics 43 (2) (2017) 257–294.

[4] J. D. Hyman, C. W. Gable, S. L. Painter, N. Makedonska, Conforming delaunay triangulation of stochastically generated three dimensional discrete fracture networks: A feature rejection algorithm for meshing strategy, SISC 36 (4) (2014) A1871–A1894.

[5] J. Hyman, S. Karra, N. Makedonska, C. Gable, S. Painter, H. Viswanathan, dfnworks: A discrete fracture network framework for modeling subsurface flow and transport, Computers & Geosciences 84 (2015) 10 – 19.

[6] H. Mustapha, K. Mustapha, A new approach to simulating flow in discrete fracture networks with an optimized mesh, SISC 29 (4) (2007) 1439–1459.

[7] A. Fumagalli, A. Scotti, An efficient xfem approximation of darcy flows in arbitrarily fractured porous media, Oil Gas Sci. Technol. – Rev. IFP Energies nouvelles 69 (4) (2014) 555–564.

[8] P. F. Antonietti, L. Formaggia, A. Scotti, M. Verani, N. Verzott, Mimetic finite difference approximation of flows in fractured porous media, ESAIM: M2AN 50 (3) (2016) 809–832.

[9] G. Pichot, J. Erhel, J. de Dreuzy, A generalized mixed hybrid mortar method for solving flow in stochastic discrete fracture networks, SISC 34 (2012) B86 – B105.

[10] G. Pichot, J. Erhel, J. de Dreuzy, A mortar bdd method for solving flow in stochastic discrete fracture networks, Domain Decomposition Methods in Science and Engineering XXI 98 (2014) 99 – 112.

[11] S. Berrone, S. Pieraccini, S. Scialò, A pde-constrained optimization formulation for discrete fracture network flows, SISC 35 (2) (2013) 487–510.

[12] S. Berrone, S. Scialò, F. Vicini, Parallel meshing, discretization, and computation of flow in massive discrete fracture networks, SISC 41 (4) (2019) 317–338.

[13] V. Girault, R. Glowinski, Error analysis of a fictitious domain method applied to a dirichlet problem, Japan Journal of Industrial and Applied Mathematics 487 (12) (1995) 317–338.

[14] S. Berrone, A. Borio, A residual a posteriori error estimate for the virtual element method, Mathematical Models and Methods in Applied Sciences 27 (08) (2017) 1423–1458.

[15] S. Berrone, S. Scialò, A. Borio, A posteriori error estimate for a PDE-constrained optimization formulation for the flow in DFNs, SIAM J. Numer. Anal. 54 (1) (2016) 242–261.

[16] G. Rozza, D. B. P. Huynh, A. Patera, Reduced basis approximation and a posteriori error estimation for affinely parametrized elliptic coercive partial differential equations, Archives of Computational Methods in Engineering 229 (15) (2008) 1886–1784.

[17] A. Quarteroni, A. Manzoni, F. Negri, Reduced Basis Methods for Partial Differential Equations An Introduction, Springer, 2016.

[18] A. Manzoni, Negri, Heuristic strategies for the approximation of stability factors in quadratically nonlinear parametrized pdes, Advances in Computational Mathematics 41 (5) (2015) 1572–9044.

[19] D. Huynh, G. Rozza, S. Sen, A. Patera, A successive constraint linear optimization method for lower bounds of parametric coercivity and inf–sup stability constants, Comptes Rendus Mathematique 345 (8) (2007) 473–478.

[20] M. Yano, A reduced basis method with exact-solution certificates for symmetric coercive equations, CMAME 287 (2015) 290—309.

[21] R. Verfürth, A posteriori error estimation and adaptive mesh-refinement techniques, Journal of Computational and Applied Mathematics 50 (1) (1994) 67 – 83.

[22] S. Berrone, A. Borio, F. Vicini, Reliable a posteriori mesh adaptivity in discrete fracture network flow simulations, CMAME 354 (2019) 904–931.

[23] S. Berrone, S. Pieraccini, S. Scialò, An optimization approach for large scale simulations of discrete fracture network flows, J. Comput. Phys. 256 (2014) 838–853.

[24] S. Berrone, S. Pieraccini, S. Scialò, Non-stationary transport phenomena in networks of fractures: Effective simulations and stochastic analysis, CMAME 315 (2017) 1098 – 1112.

25

[25] S. Berrone, S. Scialò, F. Vicini, Parallel meshing, discretization, and computation of flow in massive discrete fracture networks, SISC 41 (4) (2019) C317–C338.

[26] S. Berrone, S. Pieraccini, S. Scialò, Flow simulations in porous media with immersed intersecting fractures, Journal of Computational Physics 345 (2017) 768 – 791.

[27] M. C. Cacas, E. Ledoux, G. De Marsily, B. Tillie, A. Barbreau, E. Durand, B. Feuga, P. Peaudecerf, Modeling fracture flow with a stochastic discrete fracture network: calibration and validation: 1. the flow model, Water Resour. Res. 26 (1990) 479–489.

[28] M. Loeve, Probability Theory I, Springer, 1977.

[29] S. Berrone, S. Pieraccini, S. Scialò, C. Canuto, Uncertainty quantification in discrete fracture network models: stochastic fracture transmissivity, Comput. Math. Appl. 70 (4) (2015) 603–623.

[30] L. Dedè, Reduced basis method and a posteriori error estimation for parametrized linear-quadratic optimal control problems, SISC 32 (2) (2010) 997–1019.

[31] F. Negri, G. Rozza, A. Manzoni, A. Quarteroni, Reduced basis method for parametrized elliptic optimal control problems, SISC 35 (5) (2013) A2316– A2340.

[32] S. Berrone, S. Pieraccini, S. Scialò, Towards effective flow simulations in realistic discrete fracture networks, J. Comput. Phys. 310 (2016) 181–201.

[33] L. J. Kenneth, M. Lilia, M. Serguei, V. Rafael, Smolyak method for solving dynamic economic models: Lagrange interpolation, anisotropic grid and adaptive domain, Journal of Economic Dynamics and Control 44 (2014) 92 – 123.

[34] Svensk Kärnbränslehantering AB, Data report for the safety assessment sr-site, tech. Rep. TR-10-52, Stockholm, Sweden (2010).